MIXING DURING THE FILLING PROCESS

by

GRACE NEAL

A thesis submitted to

The University of Birmingham

for the Degree of

MASTERS OF RESEARCH

Abstract

By adapting the techniques Planar Laser Induced fluorescence (PLIF) and Particle Image Velocimetry (PIV) for a transient system with a rising free surface the mixing that occurs as a vessel is filled process has been investigated.

The PLIF technique has been demonstrated to give good repeatability for the same flow conditions and qualitative examination of the images has revealed a change in the mixing mechanism from laminar to turbulent above a critical value of the Reynolds number (Re~1000), with cases above this reaching a log variance of -2 which equates to 92% mixed. PIV allowed the distribution of momentum and shear in the tank to be investigated, highlighting dead regions in the bottom corners of the tank and showing the top half of the tank was relatively quiescent. To improve the mixing performance, changes to the flow rate and the nozzle design were made to increase the movement in these regions.

Sinusoidal variations in the inlet velocity increased the level of mixing from an unmixed state so that the vessel reached 84% mixed. With a swirl insert in the end of the nozzle the level of mixing in the tank reached 95% (log variance of -2.6) at one point in the fill. Combining these improvements may produce a more sustained and reliable improvement and should feature in any future work.

Acknowledgements

Contents

List of illustrations

List of Tables

Nomenclature

PLIF	Planar Laser Induced Fluorescence
PIV	Particle Image Velocimetry
CoV	Coefficient of Variance
TKE	Turbulent Kinetic Energy
C_i	Concentration measurement point
C_{mean}	Mean concentration
ξ_{Aij}	Reduced mean concentration
ξ_{ABij}	Contacting Parameter
k	Sensitivity exponent, strength of interation
θ	Mixing time
G_0	Greyscale when concentration is zero
G_m	Greyscale when vessel is completely mixed
G_n	Normalised greyscale
G_i	Measured greyscale values
D_M	Molecular Diffusivity
d_j	Diameter of the jet
H, h	Height of fluid in the tank
K	Intercept
M	Gradient
	Pixel size (Houcine et. al. 1996)
N	Number of sampling points
Q, q,	Flow rate (principal flow and side stream)
Re	Reynolds number
T	Tank width
D	Tank Diameter

t_D	Diffusion time
u_j, U	Jet velocity
ε	Specific energy
λ	Kolmogoroff length scale
μ:	Dynamic viscosity
v	Kinematic viscosity
ρ	Density
σ^2	Variance
L_i	Impingement height
We	Weber number
γ	Shear
x	Horizontal positon
y	Vertical position
v_x, v_y	Velocity components
σ	Surface tension

Chapter 1 Introduction and motivation

1.1 Industrial Challenge

Manufacturers will often produce a range of very similar products. This allows the product and the marketing to be targeted towards different consumer groups, increasing sales and expanding the market. There is usually a choice of colour, fragrance or flavour within each group of products so the consumer has a full range of options to cover their needs. This increased diversity has been driven by the competition and consumer demand in the market and it results in a number of challenges for manufacturing.

The shelf space available in retail outlets for each type of product has stayed constant despite increased diversity. Where previously a whole shelf would be dedicated to one product, retailers now only display a small quantity of each variety. Storing large amounts of stock is expensive and so retailers want to order small amounts of a wide range of products regularly. This in turn requires the manufacturer to either store large amounts of each variety or to make smaller batch sizes, in reality both of these have occurred.

Traditional manufacturing methods for fast moving consumer good involve production in large batches followed by filling into packaging. As the batch size required has decreased the efficiency of the production decreases due to the increase in the down time and cleaning which required between batches. The down time increases costs due to the reduction in output, the increase in cleaning produces both an environmental and financial cost due to the disposing of the waste.

A further challenge to the industry comes in the form of regulation; the European 7th Amendment Legislation means that there can be no cross contamination between fragrances above a specific low level. This is so the potential sensitizers which are contained within the fragrance are controlled in each product. Since this legislation was implemented in 2004, the level of cleaning between each batch has increased, this in turn has caused an increase in the quantity of waste generated and hence the cost associated with disposing this waste.

Changes to the manufacturing methods that would allow the flexibility to be increased would not only alleviate the increased waste and loss of efficiency, but would also provide the flexibility to react quickly to changes in the market with new products.

1.2   Late Variant Addition

To maximise the efficiency and flexibility of production, all products need to share as much of the process as possible. Products are often made using the same base fluid and a variant such as a fragrance or emotive which differentiates between the products. The aim is to find a method for mixing these variants into the base product at as late a stage as possible.

A technology that would allow the products to be mixed on the production line would reduce the waste and improve efficiency. The increased flexibility would also give the manufacturer greater ability to quickly respond to customer demand. Large amounts of stock could be released generating cash flow and also reducing storage costs.

The two major technical challenges for achieving this late variant addition are the accurate dosing of the variant and the effective mixing. In the case of personal care products the variants particularly the fragrances are usually oil based liquids which are being mixed into oil in water emulsions. The microstructure of the resulting product is greatly affected by both the quantity of the variant and the length scale to which it has been mixed. It is important that the microstructure of the product is correct as it has a large effect on the efficacy, stability and appearance and therefore customer satisfaction.

Late variant addition is already practiced by Unilever in the manufacture of their aerosol deodorants. Accurate weighing machines allow the dosage of the variants to be accurately measured and controlled; it is then mixed during the gasification of the aerosol. A similar dosing machine could be used for roll on deodorants however the mixing challenge is much greater.

There are a number of mechanisms that could provide the level of mixing required for late variant addition in roll on deodorants. These include a form of mechanical agitation such as a stirrer, mixing in the filling pipe using a static mixer, shaking or through the use of jet mixing. Of this list jet mixing would provide the most suitable solution as a stirrer or static mixer would require cleaning and shaking the product would require a large change to the filling lines which would involve a large capital expenditure.

1.3   Project objectives

Extensive studies over many years have provided a very strong understanding of mixing in large vessels; the role of impellers/agitators, recirculation through submerged jets and geometry (e.g. the effect of liquid height). However what has received less attention is the mixing that occurs as ingredients are added to vessels of small length scale, where there is no mechanical agitation. The study of such processes provides a number of experimental and modelling challenges in that start-up effects account for a significant proportion of the mixing time. There can be large disparities between the properties and ratio of the materials being added, the level of the free surface changes and the entrainment of air makes visualization difficult.

The aim of this project is to understand the mixing processes that occur during jet filling, this will characterise the range of products that can be produced in this manner. This overall goal can be broken down into smaller objectives:

- To develop the technique Planar Laser Induced Fluorescence (PLIF) to allow the level of mixing in the vessel to be measured throughout the filling process.
- Determine the parameters that set the limits for which mixing can be achieved to the required lengthscales.
- Using the technique Particle Image Velocimetry (PIV) gain an understanding of the flow structure in a filling tank
- Improve the mixing performance in the vessel

The lengthscales of the bottle to be filled are demonstrated in fig. 1.1, the flow rates range from 1.67×10^{-5} m^3 s^{-1} to 5.00×10^{-5} m^3 s^{-1}.
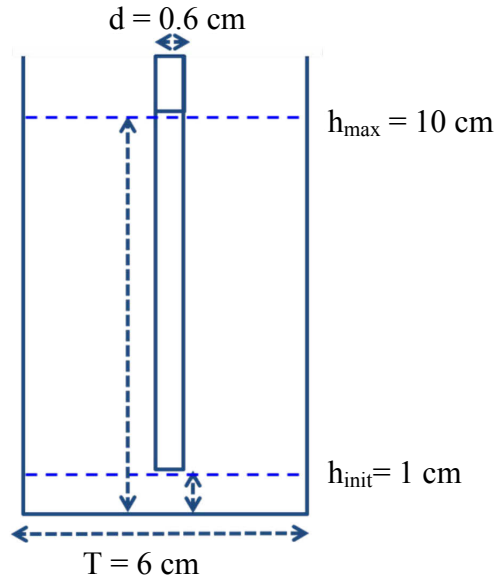
Figure 1.1. Illustration of the tank lengthscales

1.4   Thesis Layout

The first stage in this work was to investigate the available literature, this is included in Chapter 2. A full discussion of the experimental work carried out is described in Chapter 3. Chapter 4 is a description of the mixing performance in the tank with a standard straight inlet pipe while Chapter 5 goes on to examine the velocity field in the tank. Chapter 6 investigates whether improvements can be made to the mixing by using alternative pipe designs. Conclusions have been drawn in Chapter 7 along with recommendations for future work.

Work from this thesis has also been published in the archival Journal Experiments in Fluids (Neal et al.,. 2008), and presented at both the International Symposium for Mixing in Industrial Processes (ISMIP 2008) (Neal et al.,. 2008), and the World Congress in Chemical Engineering (Neal et al.,. 2009).

Chapter 2 Literature review

2.1   Introduction

Although there is little published research into the mixing that occurs as a vessel is filled there is a large body of work into mixing by a range of other mechanisms. Principles from other mixing techniques and impinging jets can be applied to the current problem and for this reason a brief outline of these are included here. Also of importance to this project is the measurement techniques which have been used to characterise the flow and mixing within the vessel: Particle Image Velocimetry (PIV) and Planar Laser Induced Fluorescence (PLIF).

2.2   Mixing

Mixing is the reduction of an inhomogeneity such as concentration, phase or temperature in order to achieve the desired process result (Paul *et al.* 2004). The quality of mixing achieved in a process can affect product quality from appearance through to the creation of microstructure, as a result an understanding of how materials mix is essential for any successful process.

The mixing mechanism depends on the flow of the fluids being mixed, turbulent flows where the velocity is constantly fluctuating reduces the scale of segregation quickly down to the size of the smallest eddies while diffusion reduces the intensity of the segregation (Kresta and Brodkey, 2004). Laminar flows do not contain the eddies seen in turbulent flow and so there is little reorientation of the fluid particles; to create mixing in a laminar flow an element of periodicity is necessary. Creating a chaotic

flow provides the stretching and reorientation required to reduce the scale of segregation (Szalai *et al.* 2004).

A large body of work has been done on a range of different mixing problems especially the flow in stirred tanks; jets have been used for mixing in a range of different situations from large storage tanks to two impinging jets on a smaller scale. Mixing in transient flows such as filling processes is less well researched.

2.2.1   Quantifying Mixing

There are a number of ways that the degree of mixing in a vessel can be quantitatively measured. The most common of these is a coefficient of variance approach defined by Kukukova *et al.* (2009) as:

$$CoV = \sqrt{\frac{1}{N}\sum\left(\frac{C_i - C_{mean}}{C_{mean}}\right)^2} \qquad (2.1)$$

Where C_i is the concentration measurement at a point, C_{mean} is the average concentration and N is the number of sample points. An alternative is to take the log of the variance as defined by Brown *et al.*. (2004). The principle of this measurement is to take the standard deviation of a measurement that indicates the concentration and determine when it has decreased to an acceptable level. The time taken to achieve this level of mixedness is called the mixing time. This has been determined experimentally within a vessel via a range of methods such as measuring changes in conductivity, pH or temperature or by looking at the mass fractions of the products from competing reactions (Brown *et al.*. 2004). Alternatively a method such as PLIF can be applied which measures changes in the optical properties of the system.

To allow the measurement of these properties a tracer is needed, this is added to the flow and causes a change that can be monitored. In the case of conductivity a salt can be used so areas of higher concentration have higher conductivity, for pH an acid will fulfil the same role. These techniques are usually measured at single points; for whole field measurements such as the optical technique PLIF a fluorescent tracer such as Rhodamine is used. When Rhodamine 6G is excited by a laser it emits light at an intensity that is directly proportional to the concentration so measurements can be made from a greyscale image of the tank. This allows a large sample of concentration values across a whole plane of the vessel, these concentrations have a distribution and this can be quantitatively analysed.

Houcine *et al.* (1996) and Fall *et al.* (2001) used a number of different statistics to analyse the concentration distributions obtained for continuously fed vessels, where a fluorescent tracer was continuously added into one feed. The first was the field of reduced mean concentration ξ_{Aij}, where the value at each pixel represents the probability of the molecules of tracer being in the volume represented by that pixel. This is calculated by dividing the mean concentration at the pixel $\overline{C}_{ij}$, obtained over a large number of samples, by the concentration in the feedstream C_{A0}:

$$\xi_{\overline{A}_{ij}} = \frac{\overline{C}_{ij}}{C_{A0}} \qquad (2.2)$$

The second statistic used was the contacting parameter, similar to the reduced concentration but where the contrast is increased, by multiplying through by one minus itself: this allows the areas of different mixing performance to be more easily identified but does not contain any new information:

$$\xi_{\overline{AB}_{ij}} = \xi_{\overline{A}_{ij}} \cdot \xi_{\overline{B}_{ij}} = \xi_{\overline{A}_{ij}} (1 - \xi_{\overline{A}_{ij}}) \qquad (2.3)$$

The third statistic was the temporal variance where the concentration at each pixel was compared with the temporal average. Houcine *et al.* (1996) proposed that the contacting parameter and the field of variance are the most important parameters to characterize, since the former gives the average state of the mixing at each point and the latter characterizes the mixing dynamics of the concentration fields. However these fields are defined by the geometry of the system so a local mixing parameter was defined as the ratio of the contacting parameter at each point to its maximum. This could be used to compare mixing performance in different mixing situations by including the pixel size *M* and a sensitivity exponent *k*. An overall parameter more sensitive to the non-homogeneous pixels was also defined and used to compare the mixing performance for a selection of different stirrers:

$$\overline{\omega} = 1 - \left(\frac{1}{M} \sum_i (1 - \frac{\xi_{\overline{AB}_i}}{\xi_{\overline{AB}_{MAX}}})^k \right)^{1/k} \qquad (2.4)$$

Fall *et al.* (2001) used a different mixing parameter to compare between systems: this was based on the difference between the concentrations of two passive tracers at each point.

$$\alpha = 1 - \left| \frac{C_A - C_B}{C_A + C_B} \right| \qquad (2.5)$$

Whilst these statistics have been designed to give a mixing criterion for continuous processes; applications of PLIF to characterise mixing in batch vessels include studies by Hall *et al.* (2004) and Chung *et al.* (2006). They determined mixing times within

small high throughput experimentation reactors by performing a log-variance analysis. The variance in this case is calculated by comparing each measured value, C_n, at a specific time with the concentration when the vessel is completely mixed, C_m, these values are normalised using the concentration before the tracer is added, C_0:

$$C_n'(t) = \frac{\left(C_n(t) - C_0\right)}{\left(C_m - C_0\right)} \qquad (2.6)$$

Feng *et al.* (2005) examined mixing in planar-jet reactors, also by measuring the variance of the intensity across the image. This statistic is also used as a mixing parameter in work by Mortensen *et al.* (2004) who examined a coaxial jet in a pipe and by Pan and Meng (2001) whose work focused on the behaviour of a tee mixer.

While CoV statistics give a measure of the intensity of the mixing it fails to describe the degree of segregation. To achieve this a measure of the structure within the mixture is required. One way to achieve this is to measure the striation thickness, as this decreases the scale of segregation has decreased, alternative methods such as that introduced by Guillard *et al.* (2000) use correlation functions to extract structural information and length scales.

Kukukova *et al.* (2009) introduced a further dimension to evaluating the mixing in a vessel which is analogous to the rate of mass transfer, it is the rate of change of segregation which they labelled the exposure, which they define as:

$$E = \sum_{1}^{N_t} \sum_{1}^{N_b} \frac{1}{2} K a_{ij} \left(C_i - C_j\right) \qquad (2.7)$$

Where N_t is the total number of measured points, N_b is the number of neighbouring points, K is the strength of the interaction and a is the contact area per side, C_i-C_j is

the concentration difference. Kukukova *et al.* (2009) state this measurement is
particularly important when the problem is dominated by the mixing timescale, such
as problems where there are mixing sensitive reactions.

2.2.2   Mixing in pipe

Jet-impaction regime

Jet-mixing regime

Wall-source regime
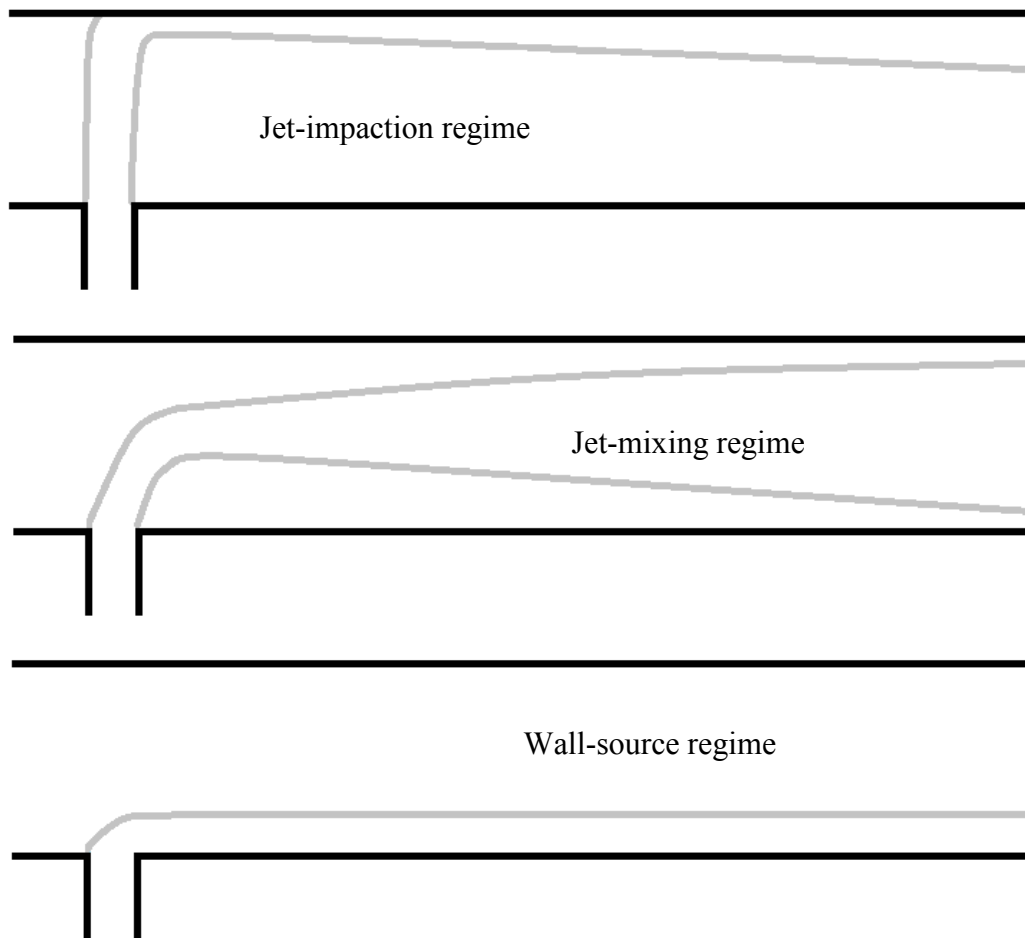
Figure 2.1 Illustration of the three different scenarios described by Pan and Meng (2001).

Pan and Meng (2001) identify three different scenarios when a jet enters a turbulent
crossflow; the jet-impaction regime, the jet-mixing regime and the wall-source
regime, these are demonstrated in Figure 2.1. In the jet-impaction regime the jet hits
the opposite wall and the large vortical structures are broken down improving the

mixing. The disadvantage of this is the stress it exerts on the opposite wall of the tee mixer.

The jet-mixing regime is when the jet penetrates the primary flow and bends until it is aligned. Turbulent entrainment creates macromixing in the pipe and the most efficient mixing in this regime occurs when the jet stream is placed so it aligns in the centre of the primary flow (Cozewith and Busko 1989). This flow has very similar flow characteristics to a jet in an unconfined crossflow (Pan and Meng 2001).

The wall-source regime is not efficient for mixing as the jet does not penetrate the pipe flow, Forney and Lee (1982) found in these cases the mixing length in the pipe (the distance downstream at which homogeneity is reached) was 50 to 100 diameters. This mixing length is dependent on the relative diameters of the two streams and the ratio of their flowrates. They came up with the optimum relation for the volumetric flow in the pipe (Q) and side stream (q) and their respective pipe diameters (D,d)

$$\frac{q}{Q} = \left(\frac{d}{D}\right)^{1.5} \qquad (2.8)$$

Pan and Meng (2001) used a pipe inlet where $6d=D$, they tested two velocity ratios v/V of 3.05 and 5.04, which give a flow rate ratio q/Q of 0.085 and 0.14 respectively. According to equation 2.8, a centred jet would be produced with a flow rate ratio of 0.068. The lower inlet flow was closer to this ideal ratio and produced an approximately centred jet, the higher flow rate was well above the ideal ratio which caused the jet to impinge on the far side of the main pipe.

While these rules apply to turbulent flows, for laminar flow, mixing will rarely occur in a tee mixer or co axial pipe inlet due to the lack of radial mixing, these flow conditions require a static mixer to enforce this radial flow (Etchells and Meyer, 2004).

2.3   Jet structure and mixing

2.3.1   Regions of an impinging jet

The structure of a turbulent jets impinging on a flat surface has been widely investigated in the literature, largely due to their use in cooling systems (Chen *et al.*, 2005). A large amount of work has been carried out looking at planar or slot jets (Law and Wang, 2000, Fondse *et al.*, 1983, Kim *et al.* 2007) but Reungoat *et al.* (2007) used PIV to measure the turbulent mixing in a round impinging jet at different impinging distances. There are three main regions used when describing an impinging jet; the free jet region, the impingement zone and the wall jet region, these are illustrated in Figure 2.2.
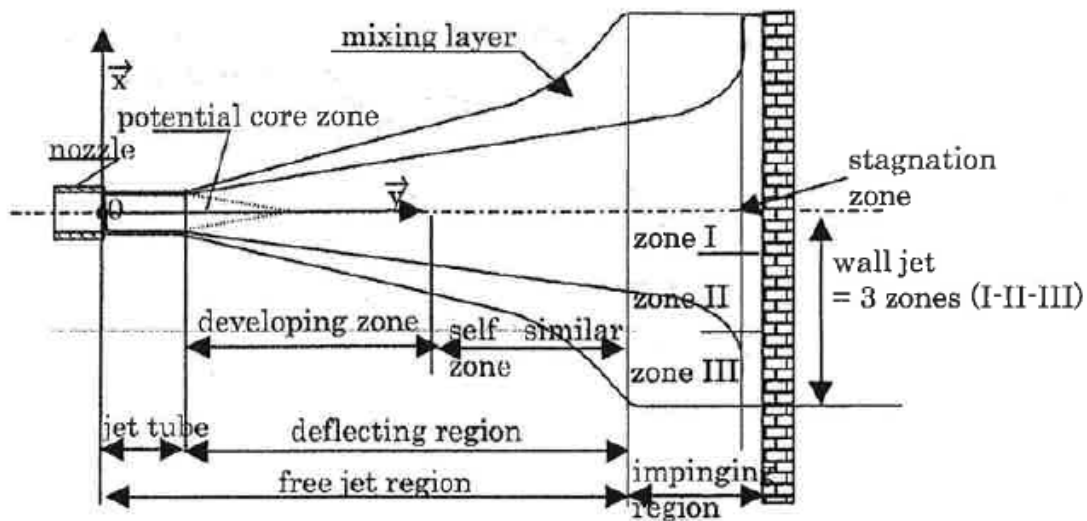
Figure 2.2 Illustration of the regions of an impinging jet, Reungoat et al. (2007).

The free jet region describes the jet between the injection point and where the impingement begins to have an effect, in this zone the jet behaves as a free jet. Near the point of injection, the momentum is maintained in the centre of the jet, this is referred to as the potential core. It was observed by Reungoat *et al.* (2007) who looked at the centreline velocity of the jet, the diameter of this core gradually decreases as the mixing layer around it expands until about 6 nozzle diameters from the injection where the jet moves into the developing zone. This agrees with Revill (1985) who stated the same relation for a free jet in an unbound bulk liquid.

In the region of 6-50 nozzle diameters, Reungoat *et al.* (2007) found the centreline velocity decreases linearly with distance, this is the developing zone and is in agreement with previous work on slot jets such as Law and Wang (2000). Fondse *et al.* (1983) describe this region as extending to 70 nozzle diameters away from the injection point where the zone of established flow or self similar zone begins. Once self similarity has occurred the cross sectional flow profile of the jet can be shown to be Gaussian (Reungoat *et al.* 2007).

In the impinging region the jet is redirected from an axial into a radial direction, this region is composed of a stagnation zone and then three wall zones (Chen *et al.* 2005). The concentration of the tracer fluid in the Reungoat *el al.* (2007) investigation appears to be high in the stagnation zone where the velocity of the fluid is low. They also observe vortical structures that roll along the wall, these are four times larger then the observed boundary layer.

The concentration distribution of a passive tracer in a jet was examined by Guillard *et al.* (1998) who used the difference between the 25% and 10% loci to determine the mixing layer. This mixing layer increased linearly away from the inlet until it reached a point 1.5 nozzle diameters from the impingement wall where the increase became exponential; this curvature was also found by Reungout *et al.* The diffusion of the jet is accelerated due to the deceleration of the jet caused by impingement on the wall. Ding *et al.* (2003) found that the concentration core in the jet decays much quicker than the velocity core of the jet, they attribute this to the faster transport of a scalar quantity such as concentration than momentum, due to the pressure gradient in the momentum transfer equation suppressing the turbulent transfer.

The studies above are all carried out on turbulent jets; Revill (1985) states that a jet is fully turbulent at Re above or about 1000-2000 and laminar for Re below 100. Kim *et al.* (2007) investigated water jets between $Re_j = 404$ and $Re_j = 1026$ and found that the jet underwent a transition to unsteady within this range. Pawlak *et al.* (2007) look at the dynamics of a starting laminar jet, the defining feature of these jets is the leading vortex ring, which is followed by a secondary vortex, behind this leading vortex pair further vortex pairs develop and grow.

The effects of the boundary layer on the mixing performance of a jet has been investigated, Ding *et al.* (2003) used PLIF with a local injection point at the edge of the jet entry to look at the mixing layer, the concentration fluctuation at each point was measured and it's maximum coincided with the area of maximum shear stress. Fondse *et al.* (1983) looked at the influence of the exit conditions on the entrainment rate and found the most important factor was whether the boundary layer was laminar

or turbulent, with laminar jets entraining 15% more than turbulent jets. Placing a grid across the outlet to promote turbulence in both the jet core and boundary layer reduced entrainment by 40%.

In all the current jet impingement studies the distance between the nozzle and the impingement wall remained constant throughout the experiment. The fluid height in the vessel was maintained using a side weir (Reungoat *et al.* 2007) or similar recirculation and the vessel was large enough that the effects of the side walls on the jet are not considered.

2.3.2   Jets in large storage tanks

Jet mixing is also found in large storage tanks where fluid from an outlet is circulated and jetted back in. Initial work on a simple system was carried out by Fossett and Prosser (1949) who were investigating underground fuel storage tanks during World War II. They proposed a relationship between the mixing time in the vessel, the vessel diameter (T), the nozzle diameter (D) and the jet velocity (U):

$$\theta \propto \frac{T^2}{UD} \qquad (2.9)$$

Although other relations have been suggested this was found to be the most accurate in a number of studies (Grenville and Nienow 2004).

 The effect of the jet angle, the vessel geometry, symmetry and aspect ratio, the nozzle diameter and the jet Reynolds number are all considered in the recent literature. One of the underpinning papers in this field is Lane and Rice (1982) who compared three different designs of jet mixing. The first was an inclined side entry jet near the base

of a flat bottomed cylinder, this design is refined to maximise the length of the jet, the second design was an axial vertical jet in a flat based cylinder, and the third was an axial vertical jet in a hemispherical based cylindrical tank. They found that the hemispherical base is the best for mixing. This is attributed to reduced stagnant areas in the bottom corners of the tank and that the liquid is constantly being redirected from the edge back into the jet.

Patwardhan and Gaikwad (2003) use a side entry cylindrical tank to investigate the nozzle angle and diameter. They use the same power input at different angles and find that the optimum mixing occurs when the jet is angled at 45 degrees to the base, they believe this is due to maximising the length of the jet so it entrains more of the surrounding liquid. The mixing is aided in this case by the outlet, which is situated in the poorly mixed bottom corner opposite the jet. The nozzle diameter is also varied; they found that increasing the diameter improves the mixing at the same power consumption.

The effect of jet angle can be modelled using computational fluid dynamics (CFD). Zughbi and Rakib (2004) used FLUENT with a tetrahedral mesh for their simulations, they validated their results using the experimental results of Lane and Rice (1982). They used the temperature rather than the concentration to measure the mixing time, it was assumed that density and viscosity were constant over the temperature range used so that the flow properties are unaffected. Their results showed that the optimum angle is around 30 degrees to the base of the tank for entry at the base. This appears to disagree with the theory presented originally by Lane and Rice that the optimum mixing occurs when the jet length is maximised.

A theory to explain the results was suggested in a following paper (Zughbi and Ahmad 2005). It states that the jet length does need to be maximised but this does not necessarily occur at 45 degrees. The jet may have dissipated before reaching the opposite corner, however if the jet is deflected off the opposite wall a greater jet length is achieved. This theory agrees with the evidence from tee mixer experiments where the mixing is also improved though deflection of the jet.

2.3.3   Impinging jets

Studies have also been carried out on the mixing that occurs between two impinging jets. The work by Unger and Muzzio (1999) investigates the two different geometries for mixing jets shown in figure 2.3. Low Reynolds number jets (Re < 80) were better mixed in the asymmetric geometry this was due to the swirling motion created, little mixing occurred when these jets were fired directly at each other. For unsteady laminar flows (80 < Re < 300) the symmetrical geometry created better mixing, this was thought to be due to the oscillations in the jet streams which are more effective at mixing than the swirling nature of the flow in the asymmetric case. High Reynolds number jets were effectively mixed in both geometries although the asymmetric case was more efficient as it reduced the dead zones in the vessel.

(Standard Geometry)   (Asymmetric Geometry)
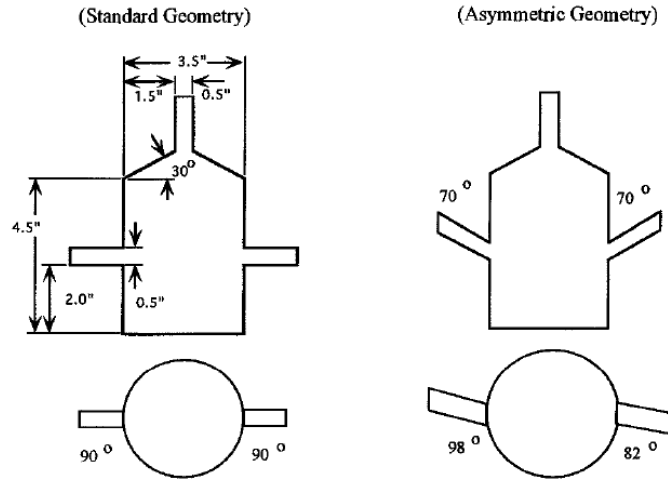
Figure 2.3 (Unger and Muzzio 1999) Geometry of the impinging jet mixers.

2.4 Mixing and flow diagnostics

Mixing and flow diagnostic techniques can be either single point or whole field measurements. Single point measurements detect the instantaneous flow velocity or concentration at a fixed point at a defined frequency in time, while the whole field techniques measure over an entire area or volume at an instant in time, examples are given in table 2.1.

	Single Point	Whole field
Velocity Field	Hot wire anemometry (HWA), Positron Emission Particle Tracking (PEPT), Laser Doppler Velocimetry (LDV), Computer Automated Radioactive Particle Tracking (CARPT)	Particle Image Velocimetry (PIV), Magnetic Resonance Imaging (MRI).
Concentration	Conductivity, pH or temperature probes	Planar Laser Induced Fluorescence (PLIF), mass fractions of the products from competing reactions

Table 2.1 Measurement techniques

The techniques relevant to this work are the optical techniques of PLIF and PIV, this review is focused on these two methods.

2.4.1   PLIF

Planar Laser Induced Fluorescence (PLIF) is a technique based on the measurement of the instantaneous concentration distribution of a fluorescent material in a specific plane. To relate the intensity of the fluorescence of the tracer to its concentration it is important that there is a linear relationship between them; this is the case for dilute tracers and is verified and calibrated before each study. PLIF has been used as a technique in a number of different application areas including combustion of gases (Hult *et al.,* 2005; Degardin *et al.,* 2006; Weigand *et al.,* 2006), flows of liquids in vessels (Hall *et al.,* 2004; Dazin *et al.*, 2006) and impinging liquid jets (Unger *et al.,* 1999).

Analysis of the data obtained from PLIF analysis requires the creation of a matrix of greyscale values from the black and white digital images obtained, this matrix is then used to compute various statistics such as those outlined in section 2.2.1. Due to the large amount of data to be handled, analysis using computation is essential. The use of the software package, Matlab$^{®}$ to analyze the results was investigated by Golnabi (2006) who described how Matlab can be used to import and convert an image into a two dimensional array with values based on the intensity of the image data at each pixel.

There are a number of error sources in PLIF measurements, mainly associated with the optics, camera sensitivity, the Gaussian distribution of the laser intensity and temporal laser fluctuations. Golnabi (2006) used a continuous flow at a constant concentration illuminated from the side by a Nd:YAG laser, the signal was then

averaged along each row and column. The signal intensity was found to decrease linearly across the cell, which was attributed to a decrease in camera sensitivity away from the centre of the image. The errors that occur in PLIF images were also analyzed by Law *et al.* (2000) who state the importance of the perpendicular positioning of the camera relative to the light sheet to avoid deformation in the images. The unsteadiness of the laser sheet was also measured in this study by sampling 32 frames of uniform concentration; they found the maximum standard deviation for individual pixels to be 2 grayscale units on an 8 bit (256) grayscale, which was determined to be insignificant.

The above studies show that there is a body of work on the application and validation of PLIF to obtain an understanding of mixing in *steady* flows with minimal free-surface disturbance. However, the use of PLIF to gauge mixing performance in *unsteady* (time-dependent) flows with moving free-surfaces has received very little attention.

2.4.2   PIV

Particle Image Velocimetry (PIV) is a whole field visualisation technique which yields an instantaneous velocity field obtained over a short time interval over a given flow area of interest. This is achieved through measuring the displacement of particles within a thin laser sheet. PIV is non intrusive, indirect velocity measurement technique has developed rapidly recently with the improvements in cameras lasers, optics and software (Raffel *et al.* 2007).

The PIV technique is demonstrated in Figure 2.4   This area of interest is illuminated by a laser sheet and images of this sheet are captured using a camera. Each image is

then split into a grid of interrogation windows and statistical techniques are used to

assign a velocity vector to each window.
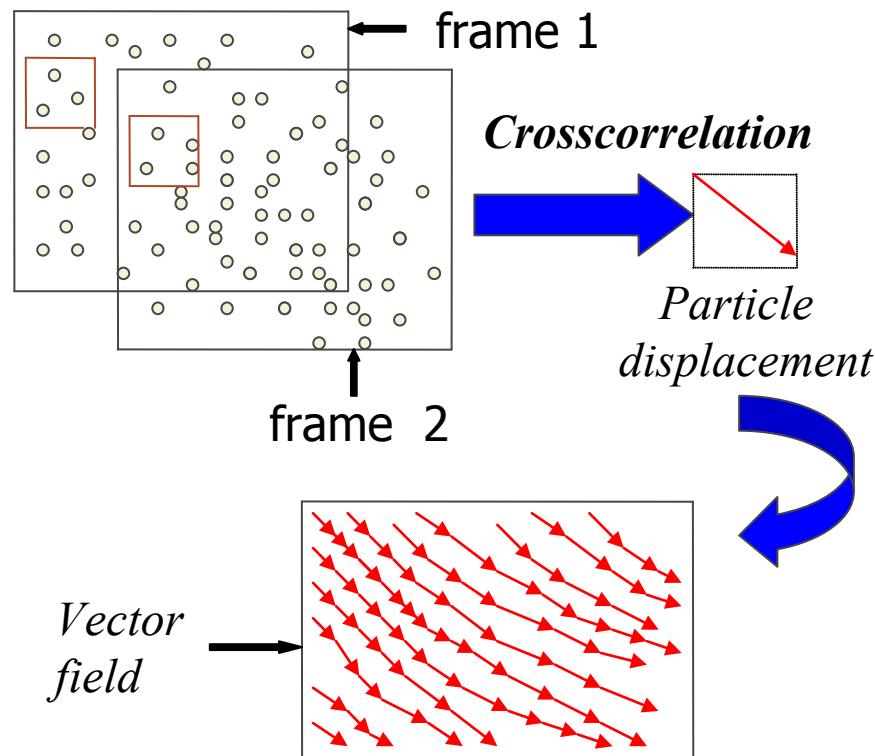
Figure 2.4 PIV analysis

Pawlak *et al.* (2007) look at the dynamics of a starting laminar jet using a dynamic

particle image velocimetry (DPIV) system and PLIF. The DPIV system uses cross

correlation to produce a coarse grid of velocity vectors, filters this to remove outliers

then a fine grid analysis is performed, the resulting velocity field is filtered again

using a threshold median filter to eliminate outliers. The individual velocity fields are

then presented alongside the PLIF images for this transient process. Six different

integrals are calculated in the region of the leading vortex, the first is proportional to

the axial momentum flux exiting a disc perpendicular to the axial direction, the

second is related to the flux of vertical momentum and the third is responsive to radial

velocity changes. These three integrals are used to determine the exact axial location

of the vortex and a further three similar cases are used to determine the radial position. The vorticity of the vectors was also used to analyse the local recirculation in the vortex.

Turbulence is where there are temporal fluctuations in the fluid velocity at any point, this can be measured through the PIV technique. It is assumed that the instantaneous velocity can be decomposed into an average velocity and a fluctuating part. This fluctuating part is usually characterised through an RMS value, the turbulent kinetic energy (TKE) is the portion of the kinetic energy that is due to these fluctuations. As PIV measures the velocity in a plane the third dimension is estimated from the two dimensions in the frame by assuming the turbulence is isotropic. Saarenrinne *et al.* (2001) states that the spatial resolution needed to capture 90% of the turbulent energy is twice the Kolmogorov scale however Chung *et al.* (2006) obtain 95% accuracy with a lengthscale of 20 times the Kolmogorov lengthscale.

Turbulent Kinetic Energy is a common statistic used in the analysis of turbulent jet flow (Weisgraber and Liepmann, 1998, Bi *et al.,* 2003,) however it may not be possible to perform this on a transient flow, other analyses performed on a turbulent jets include proper orthogonal decomposition. Bi *et al.* (2003) used DPIV and proper orthogonal decomposition (POD) to determine the coherent structures in the flow. The principles behind this involve maximising the correlation between the flow description and the experimental results from the PIV, this is done by finding the eigenmodes of the flow. They captured the velocity field at a frequency of 1000Hz, using this data they plotted the spectral density of the frequency of the velocity fluctuations in the centre of the shear layer on one side of the jet and found that the

preferred frequency of the fluctuations was approximately 11Hz. The PIV images were then grouped into 80 blocks each containing 256 files giving a bandwidth of 3.9Hz, these were then analysed using POD, they note that the first six spatial eigenmodes capture over 50% of the energy, lower than in traditional turbulence as more eigenmodes were needed to capture the higher number of degrees of freedom of turbulence caused by carrying out the analysis in the streamwise direction and in the temporal domain. Kim *et al.,* (2007) state that the eigenvalue represents the energy of each eigenmode, they note that the proportion of energy in the first six modes increases as the Reynolds number increases, which implies the flow has lower dimensional structures.

2.5   Summary

Although there is little published research into the mixing that occurs as a vessel is filled there is a large body of work into mixing by a range of other mechanisms. This mixing is measured in a variety of ways from full field techniques such as PILF to single point measurements of concentration and is often quantified using a coefficient of variance statistics. From studies on mixing involving jets it can be seen that the mixing performance improves if the length of the jet, including any impinged flow, is maximised.

The techniques PLIF and PIV have been used to measure a variety of flow scenarios, however in most cases the system is a steady state. There has been no study of transient systems with a moving free surface, this work will adapt these techniques to measure the mixing in this case.

Chapter 3 Materials and Methods

3.1   Introduction

A number of experiments were carried out throughout the project to determine the flow properties and mixing performance for filling systems. Initially work was done using a square section tank and a stationary pipe, this was then modified so that the pipe could retract above the surface of the fluid. In both cases experiments were carried out using PLIF and PIV to determine the level of mixing and the velocity field respectively. Parameters such as nozzle design and flow rate were adapted based on these results and the modifications were examined experimentally.

3.2   Mixing tank

3.2.1   Dimensions and equipment set up for static pipe system

A schematic of the experimental set-up is shown in Figure 3.1. The vessel used was a $T = 0.06$ m square section tank; the square shape was chosen to eliminate any errors due to refraction through curved surfaces. The fluid enters the tank through a 0.006 m diameter vertical dip pipe aligned with the central axis of the tank. The tank was filled to a height, H, of ~ 0.1 m ($H/T = 1.67$). A digital dispensing gear pump (MicroPump 75211-35, Cole-Palmer USA) was used to produce a continuous pulse-free flow. The volumetric flow rate of the pump was calibrated to the pump speed (controlled digitally) for each viscosity of fluid used using the bucket and timer method. Additional checks on the flow rate supplied by the pump were made by monitoring the rise in liquid level in the tank as a function of time.

2626
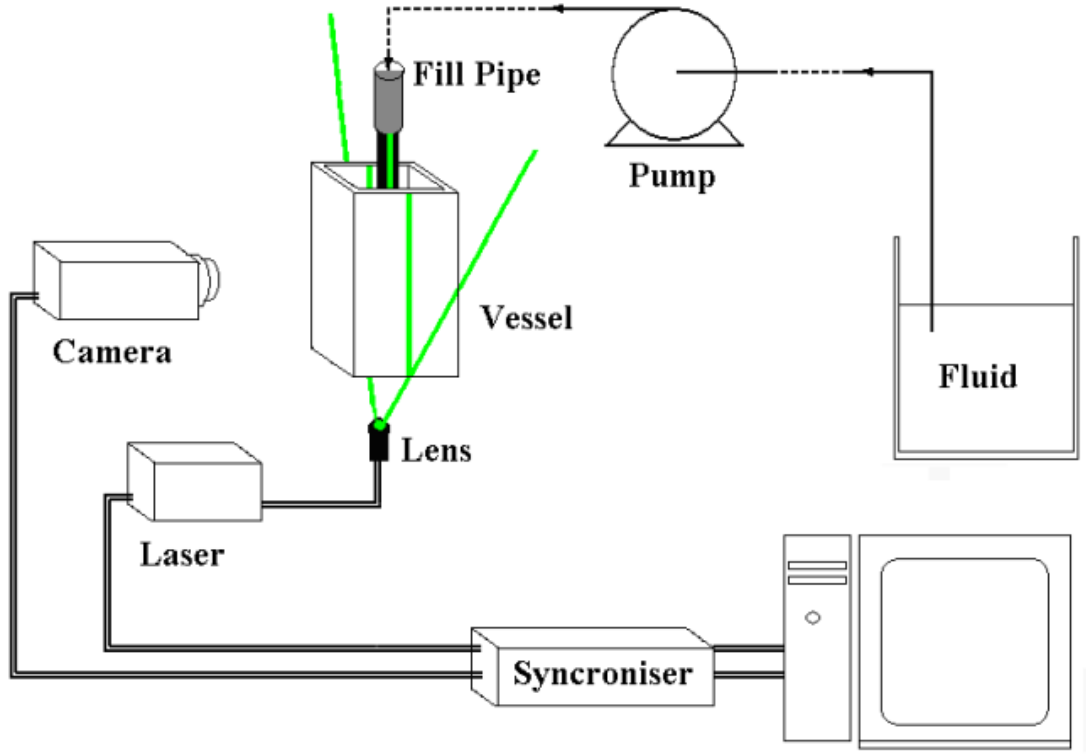
Figure 3.1 Schematic of the experimental rig and PLIF set up.

3.2.2   Moving nozzle set up and control

Entrainment of air in the jet causes bubbles to be formed in the tank, when the laser sheet hits these bubbles it is scattered causing shadows in the plane of interest. Bin (1988) calculated the impingement height of the jet L_j for which air entrainment begins in the region where the plunging jet would split into individual droplets region as:

$$\frac{L_j}{d_0} = 1.4 \times 10^{-5} d_0^{-1.79} We_j^{0.937} \qquad (3.1)$$

Where We is the Weber number which is calculated from the density (ρ) the velocity (v), the lengthscale (l) and the surface tension (σ):

$$We = \frac{\rho v^2 l}{\sigma} \qquad (3.2)$$

This gives an approximate value of L_j as 16 cm for the highest velocity fluid used in these experiments, however in the continuous jet region entrainment will occur at a shorter length. Whether the jet is in the continuous or droplet regions is dependent on the inlet turbulence parameters. Initial test cases demonstrated air entrainment when the pipe was fixed above the maximum fill level of 10cm, an impingement height of 3cm prevented most entrainment however a pipe fixed in this position would quickly become submerged. To allow the jet to impinge on the surface of the fluid while preventing the impingement height from exceeding this limit the nozzle was raised so it stayed just above the level of the fluid in the tank.

To adapt the filling set up to allow the pipe to be moved, a purpose built traverse was designed (Figure 3.2) which allowed the pipe to move in the vertical direction at a controlled speed and with minimum vibration. This consisted of a motor which rotated a vertical screw thread along which the pipe moved guided by two supports. The speed was controlled using a specifically written control program and was manually set before filling began. This speed was chosen to be the same as the rate at which the free surface rose which was calculated from the flow rate. The rig included cut off switches positioned to limit the pipe's range of movement to keep it within the range of the screw and also to prevent it from colliding with the vessel. The traverse was started manually at the beginning of the filling process to coincide with the initialization of the pump.
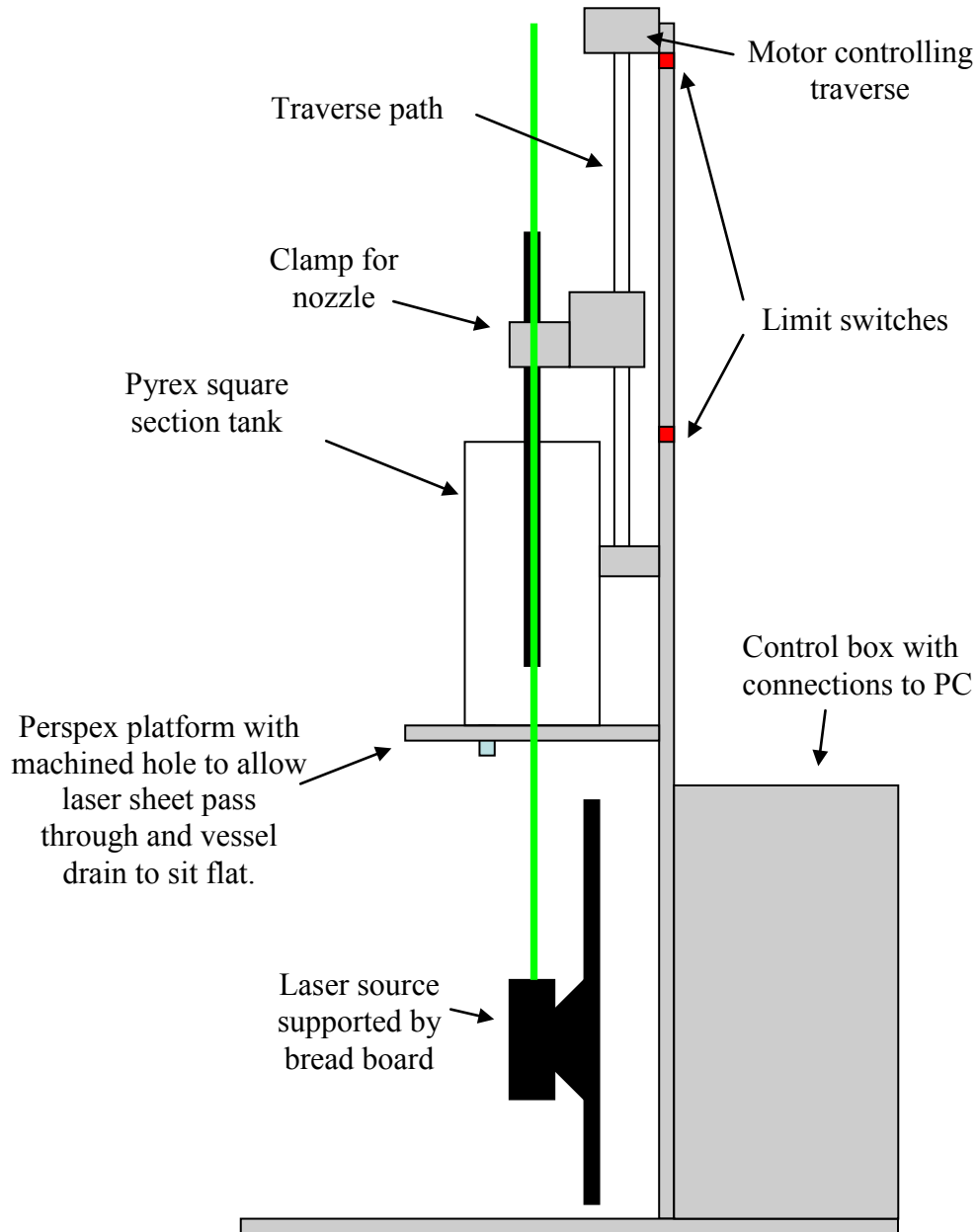
Figure 3.2 Schematic of the nozzle traverse.

3.2.3   Set up of case studies

A number of improvements to the system were investigated experimentally. These

improvements fell into two groups; varying the flow rate and changing the pipe

geometry.

A variable flow rate was created using a computer program to control the pump, this was written by Andrew Tanner from the Biosciences Workshop at the University of Birmingham. The program was written so that an excel file read the time and the flow rate and any function that could be written in excel could be used to describe the flow, the program then runs until it reaches an empty cell, at this point the pump is stopped. The actual flow rate achieved is fed back to the computer and is displayed graphically alongside the prescribed function this can then be exported to excel. Due to limitations of the pump there was a lead time between the function and the actual speed achieved and depending on the desired flow rate there was a certain length of time to start up. This could be up to 2.5 seconds for the highest flows which meant that there was a limit on the rate of change of the flow. For a sinusoidal function the period achievable was 4 seconds, the flow rate was varied from $1.67 \times 10^{-5} \, m^3 \, s^{-1}$ to $5 \times 10^{-5} \, m^3 \, s^{-1}$. For the ramped flow the flow rate started at zero and accelerated up to the highest rate of $6.67 \times 10^{-5} \, m^3 \, s^{-1}$. In both cases the average flow rate was $3.33 \times 10^{-5} \, m^3 \, s^{-1}$.

Three nozzle designs were made to improve the mixing in the tank, two of these had cone inserts in the base and one had a 'swirl' insert. For the cone insert the pipe was flared to accommodate it, as shown in Figure 3.3, in practice spot welds were required to attach the inserts to the outside of the pipe. The swirl nozzle was created by inserting and welding a twisted piece of metal into the end of the pipe.
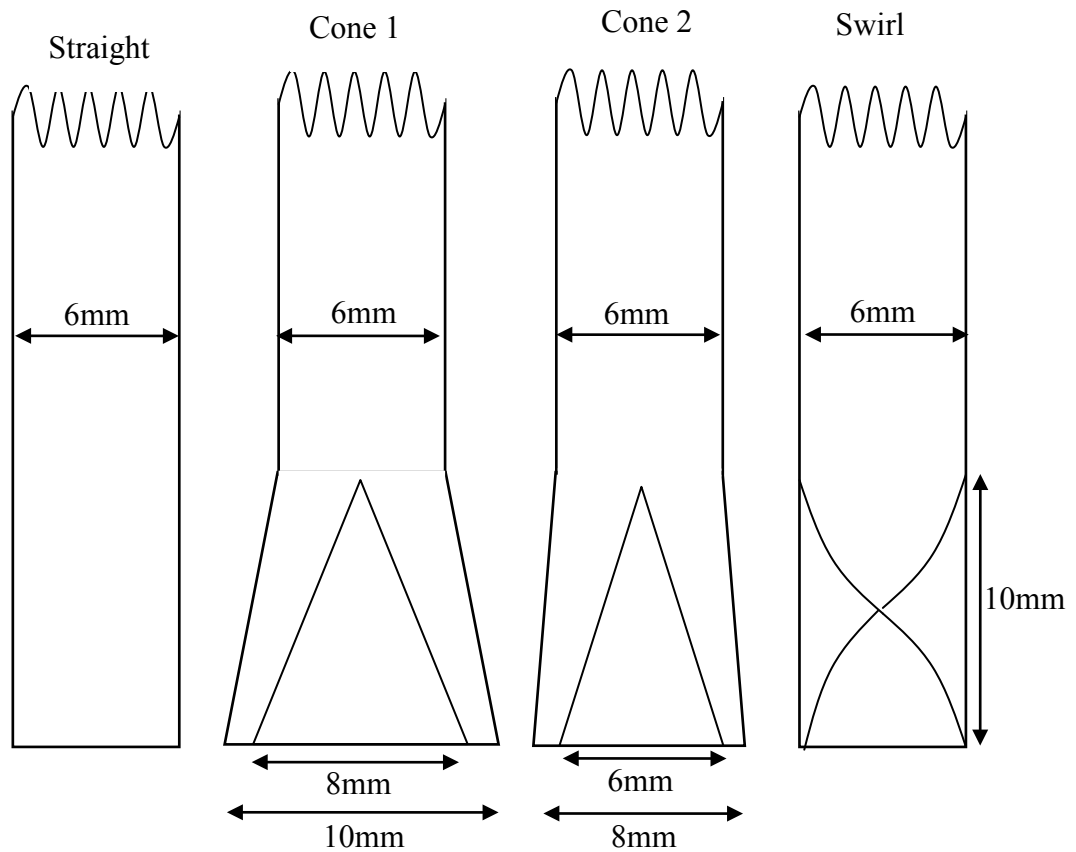
Figure 3.3 Schematic of a straight pipe and the three nozzles improvements.

3.3   Fluid properties

3.3.1   Newtonian Fluids

The experiments were carried out using Newtonian fluids. It was necessary for the fluids to be transparent to allow the laser beam to pass through for the PLIF and PIV diagnostic techniques. Aqueous glycerol solutions were chosen for initial studies, with viscosities ranging from 0.003 Pa s to 0.016 Pa s measured using a rheometer equipped with a cone and plate geometry (TA AR1000, TA instruments). The fluid properties are described in Table 3.1

Flow rate, Q (m³ s⁻¹)	Fill time, t (s)	Energy dissipated, ε (W kg⁻¹)	Stationary pipe experiments				Moving pipe experiments			
			Viscosity, μ (Pa s)	Density, ρ (kg m⁻³)	Reynolds number, Re (-)	Kolmogoroff length scale, λ (μm)	Viscosity, μ (Pa s)	Density, ρ (kg m⁻³)	Reynolds number, Re (-)	Kolmogoroff length scale, λ (μm)
1.67×10^{-5}	21.6	0.008	3×10^{-3}	1056	1245	231	4×10^{-3}	1081	956	282
			6×10^{-3}	1121	661	389	8×10^{-3}	1126	498	459
			12×10^{-3}	1164	343	654	16×10^{-3}	1170	259	751
3.33×10^{-5}	10.8	0.064	3×10^{-3}	1056	2490	131	4×10^{-3}	1081	1911	168
			6×10^{-3}	1121	1322	221	8×10^{-3}	1126	996	273
			12×10^{-3}	1164	687	372	16×10^{-3}	1170	517	446
5.00×10^{-5}	7.2	0.217	3×10^{-3}	1056	3735	94	4×10^{-3}	1081	2867	124
			6×10^{-3}	1121	1983	158	8×10^{-3}	1126	1494	202
			12×10^{-3}	1164	1030	266	16×10^{-3}	1170	776	329

Table 3.1 Experimental parameters, where Reynolds number is defined as $\mathrm{Re} = \dfrac{\rho d_j u_j}{\mu}$.

3.4   *Planar Laser Induced Fluorescence (PLIF)*

PLIF images were obtained using a TSI Powerview system (TSI Inc. USA)
comprising of a single 1000×1016 pixel, 8 bit Charged Coupled Device (CCD)
camera (TSI PIVCAM 10-30, TSI Inc, USA), synchroniser and a dual head Nd-Yag
laser emitting at 532 nm (New Wave Inc., USA) and equipped with laser sheet optics.
The lenses used were a -15 mm cylindrical lens and a 200 mm spherical lens and the
laser was positioned 150 mm from the base of the vessel; this combination was
chosen so that thickness of the sheet was a minimum in the middle of the vessel. The

laser sheet thickness throughout the imaging plane was less than 1 mm. The system was controlled using a Dell Precision 620 workstation (Dell Corp. USA) running INSIGHT 6.0 software. The images were captured at a rate of 15 Hz, saved as .tif files and exported to the Matlab software for analysis.

The fluorescent tracer used was Rhodamine 6G which emits light at 566 nm when excited using radiation at 532 nm, Rhodamine was chosen as the relationship between the concentration and the intensity of the laser light emitted and hence the grayscale of the images is linear over a certain range of concentration, this is known as the Lambert-Beer law. This linear relationship was measured for different concentrations, this was carried out at two different laser intensities; the graph obtained is shown in Figure 3.4. The linear relationship of concentration is seen to hold up to a concentration of 0.0001 kg m^{-3} (0.1 mg L^{-1}) and of the two laser intensities used the higher gave a better resolution over the required range and was therefore used for the experiments. Before the fluid injection began 1×10^{-6} m^3 of the tracer was spread across the bottom of the vessel, as this tracer is then diluted by the inflowing fluid the concentration of the tracer was chosen so that the concentrations in the vessel would be within the linear range when the level of mixing was being measured. Measurement took place when the fluid level reached approximately 2 cm until the vessel was full, this meant the tracer would be diluted by a factor of 100 before measurement took place, so the concentration used was 0.008 kg m^{-3} (8 mg L^{-1}), as this would ensure that the concentration was within the linear region before measurement began. The camera was fitted with a sharp cut-off high-pass wavelength filter of 545 nm (ALP545, TSI Inc.) to eliminate the light from the laser at

532 nm and allow only the fluorescent light from the tracer fluid at 566 nm to pass through.
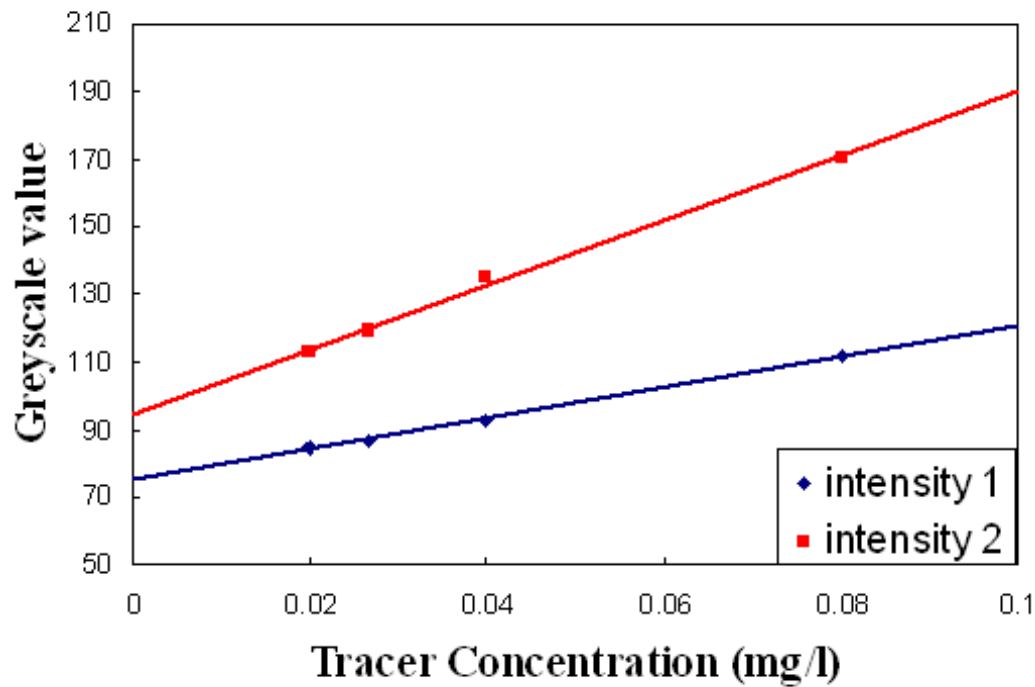
Figure 3.4 Plot of greyscale as a function of tracer concentration at two different laser intensities.

3.4.1   Normalisation

As shown above, the relationship between the measured grayscale values and the tracer concentration was found to be linear throughout the concentration range found when the fluid heights were above 2 cm. To determine this linearity precisely a set of images must be taken to calibrate the grayscale values measured for each pixel in the image to the tracer concentration.

There are two main considerations to take into account when determining the pixel by pixel values of concentration from the grayscale values; the laser sheet intensity has a Gaussian profile across the plane so a uniformly mixed tank will not emit a uniform

intensity of light, and the individual pixels of the CCD array in the camera do not have a uniform sensitivity. To eliminate these sources of error each pixel is calibrated independently. This is accomplished by taking 50 pictures at one known concentration with the vessel fully mixed; this process is then repeated with double the known concentration. The average grayscale value for each pixel over the 50 images is then calculated at each concentration and hence two arrays containing the pixel by pixel values of grayscale are created. The linear relationships connecting the corresponding pixel by pixel values of greyscale with concentration in the two matrices are determined and a further two matrices are created containing the gradient (M) and intercept (K) of these linear equations. This is demonstrated in Figure 3.5 using the first two pixels as examples, the nth element of the M or K matrix is calculated from the measured greyscale at the nth pixel of the image when the concentration is x and the greyscale when the concentration is $2x$.

The zero concentration case is not used in the calibration as it does not include the error associated with any non-uniformity in the laser sheet. This is because with no concentration there is no fluorescence is emitted which the only detection method for the local intensity. However they do allow the level of this variation to be quantified. If the linear relationship obtained from two non-zero concentrations is extrapolated back to the zero point there is found to be an error of 2.26 % between the calculated 'K' values and the experimental greyscale values for an image of an illuminated vessel with no tracer.
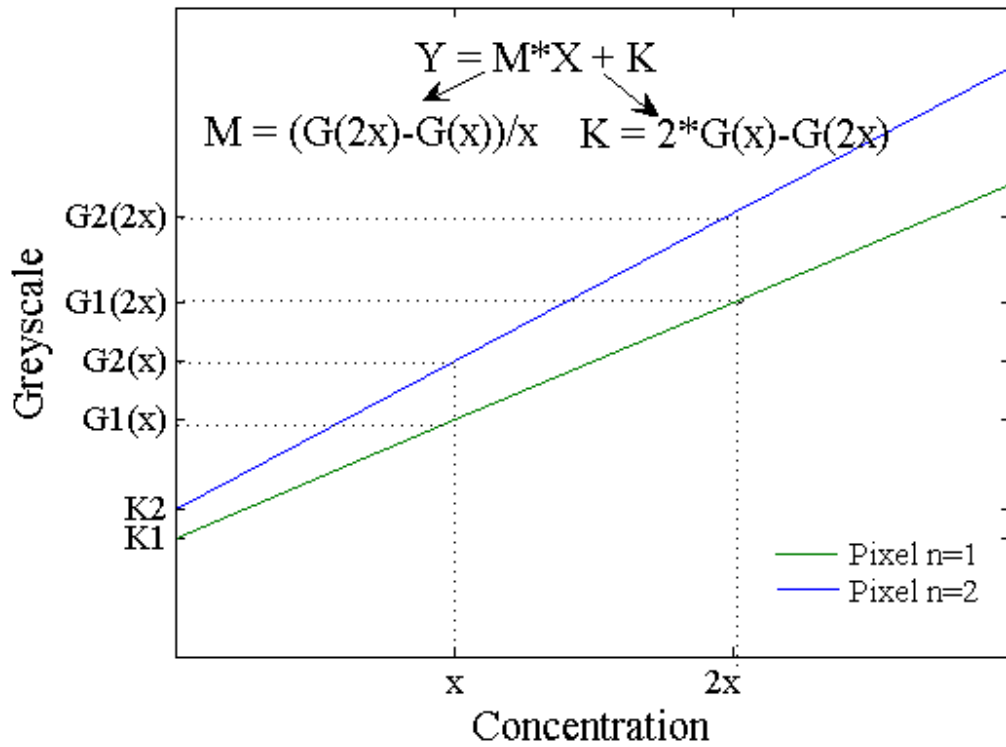
Figure 3.5 Calculation of elements of the matrices M and K from the linear relation between greyscale and tracer concentration for each pixel, (only two pixels are plotted for demonstration).

Each image is then loaded one at a time into Matlab as an array of greyscale values (see appendix for sample code). The image is then cropped so that only the area of the image containing fluid is analyzed. The surface of the fluid is located by calculating the average of each row and determining when this average is more than 10% higher than the background grayscale, the first point at which this is the case is taken to be the free surface of the fluid. This was checked and found to be the best cutoff by viewing cropped images to ensure that the fluid area had been correctly identified, the calculated height of the fluid is also monitored to ensure it increases linearly throughout the filling processes. If the height does not increase steadily with image number then the images are not accurate and are discarded, this occurs when a droplet forms on the pipe of edge of the tank which reflects the light higher in the

vessel. For the purposes of this analysis the image is split into two interrogation zones, one on each side of the inlet pipe. The change in the average greyscale values at the surface and the area used for the analysis are shown in Figure 3.6.
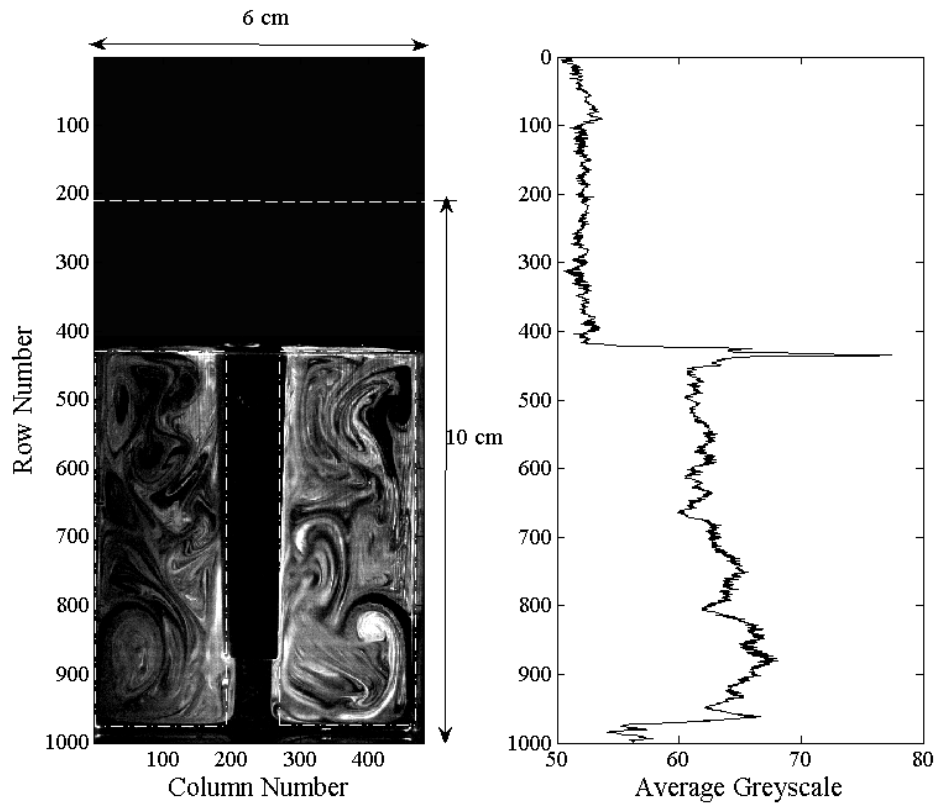
Figure 3.6 Definition of the location of the fluid surface via the change in the average row greyscale values as a function of the vessel height. The interrogation zones are shown and also the maximum fill height.

The height of the liquid in the vessel is then calculated from the number of pixels that cover it using a scaling factor calculated using the base of the tank as a standard distance, and from this the average concentration of the fluid in the vessel at that height. This is then converted into a grayscale value (G_n) at each pixel using the calibration matrices. The average concentration in the vessel is the concentration each pixel would be at if the vessel were fully mixed; it is dependent on the fluid height in the vessel, the concentration of the tracer and the volume of tracer used.

This concentration decreases as the vessel is filled which means that the degree of

mixing is being measured against a coarser scale when the vessel is nearly full.

3.4.2   Log variance and image analysis

To obtain the degree of mixedness in the vessel as a function of height a log-variance

analysis is used as described by Brown *et al.* (2004). The grayscale value at the nth

pixel is normalized at each time *t* by considering the grayscale values when the

concentration is zero i.e. background (G_0) and the value if the vessel was completely

mixed at that fluid height (G_m);

$$G_n^{'}(t) = \frac{\left(G_n(t) - G_0\right)}{\left(G_m - G_0\right)}, \qquad (3.3)$$

where G'_n (t) is the normalized grayscale value and G_n (t) is the grayscale value of the

n^{th} pixel in an image taken at a time t. The log-variance (σ^2) of the concentration in

the interrogation area is then calculated, this is defined as;

$$\log \sigma^2 = \log \frac{1}{N} \sum_{n=1}^{N} \left(G_n^{'} - 1\right)^2, \qquad (3.4)$$

where *N* is the total number of pixels used in the image. The log-variance gives a

direct measure of the level of mixing on the scale of a single pixel and as the mixing

improves this number decreases. For example, when the vessel is 95% mixed the log-

variance is log $(1 - 0.95)^2$ = -2.6.

The number of pixels included in the variance increases with the height of the fluid

due to the larger area covered, this causes the error in the measured log variance to be

reduced though the process as the sample size increases. However the scale of the

mixing being measured does not change throughout the fill, for this to be reduced a higher resolution camera would need to be employed.

In order to ensure that the equipment has sufficient resolution to resolve mixing events across all the length-scales, a characteristic length scale equivalent to the Kolmogoroff scale for turbulent mixing was calculated. Although the mixing mechanism was shown later to be predominantly laminar for the higher viscosity fluids, hence the Kolmogoroff scale would not be expected to apply, calculation of this scale provides an order of magnitude check on the likely accuracy of the technique. The Kolmogoroff length scale is a function of the energy input per unit mass to the fluid, ε, and the kinematic viscosity of the fluid, v:

$$\lambda = \left(\frac{v^3}{\varepsilon}\right)^{1/4} \qquad (3.5)$$

In a filling system, if the fill rate is constant, the mass of fluid in the vessel increases linearly in time. The energy input per unit mass to the fluid from the liquid jet was calculated on the basis of the dissipation of the kinetic energy into the bulk fluid in the fully filled vessel; this provides the minimum value of specific energy, ε, input during the filling process,

$$\varepsilon = \frac{\frac{1}{2}\rho Q u_j^2}{\rho T^2 H}, \qquad (3.6)$$

where Q is the volume flow rate of liquid, ρ is the density, u is the velocity of the jet and T and H are the height and width of the tank.. Values of λ and ε, calculated using (*3.5*) and (*3.6*) respectively are given for each experiment in Table 1. The range of λ is from 94-650 μm, this compares well with a pixel by pixel resolution in the images of 130 μm.

3.4.3 Calibration and error

Using the calibration method, the pixel by pixel variations in the laser sheet and in the camera sensitivity are taken into account, however, this analysis assumes that the intensities within the laser sheet are constant each time the laser head is triggered. The fluctuation in the laser sheet with time was examined by observing multiple calibration images. The concentration and liquid height were kept constant for 50 images so that temporal fluctuations in the signal could be attributed to the laser. The laser sheet fluctuation had an average standard deviation of 2% for each pixel. This error propagates through the calculations, there will be a 2% error in the two intensities used to calculate the values of M and K, giving a 2.8% error in each pixel. These are in turn used to calculate the fully mixed concentration and the normalized concentration. Despite this propagation of error the large number of pixels used for each log-variance value reduces the error. If more than 120 pixels are used it is reduced to below 1% giving an error due to laser fluctuation in the log value of less than 0.004, for a full vessel more than 15000 pixels can be used.

A further cause of anomalous concentration results occur when there are pixels which have very low sensitivity or have been damaged. When the difference between the grayscale value at zero concentration, G_o and at the fully mixed condition, $G_{m,}$ is too small, their use in the denominator of Equation *3.2*, leads to a very coarse measurement which is not statistically significant. Any damaged pixels in the camera appear as permanently saturated with light so the differences between the grayscale values from these pixel is zero, this means that when the concentration values are normalized an infinite answer is obtained. To eliminate both these problems all pixels where the difference between the concentration at zero and the concentration at fully

mixed is less than a certain cut off value, usually taken as 10 are discarded prior to taking the log-variance.

3.5   *Particle Image Velocimetry (PIV)*

PIV images were obtained using a TSI high-speed PIV system. A high repetition rate laser (10mJ at 1kHz) was used for illumination (New Wave) and a high frame rate camera (Photron APX RS) to capture data at 500 Hz with a spatial resolution of 1025 $\times$ 1025 pixels^2. The lens set up used was identical to that used in the PLIF experiments described above.

The particles used to trace the fluid were silver coated glass particles of diameter 10 μm which reflected the light at the same wavelength as the initial laser plane (532 nm). These particles have a sufficiently small relaxation time that they can be assumed to be following the fluid motion; they were well mixed into the fluid before the injection of the fluid into the vessel during the experiment. The instantaneous spatial displacement of the particles in the vessel was calculated by splitting the images into small interrogation windows 32x32 pixels. Fast Fourier Transform and Gaussian statistics were then used to cross correlate between the images from the two time exposures. The spatial displacement that produces the maximum cross-correlation statistically approximates the average displacement of the particles in the interrogation window (Hall *et al*. 2005). The velocity of the particles can then be calculated by combining this information with the known pulse separation. The resulting matrix of velocity vectors defines the instantaneous flow field in the whole image.

The resolution of the velocity field measured using the PIV is dependent on the magnification of the camera, the size of the interrogation window and the pulse separation. The optimum pulse separation is calculated by defining the maximum displacement between the pulses as one quarter of the interrogation window. The amount of particles in each interrogation window also affects the accuracy of the cross correlation, the optimum seeding for the fluid is 10-12 particles per interrogation window.

3.5.1   Assumptions and analysis techniques

To obtain an accurate picture of the flow it is necessary to average over a number of images, however in a transient flow this is not possible. An assumption that the fluid height was stationary throughout the capture of 200 images was made so that averaging could be used. The time needed to capture 200 images was 0.4 sec, for the worst case scenario, a flow rate of 5.00×10^{-5} m^3 s^{-1} the fluid height changed by 0.0056 m in this time; for the assumption to be valid the flow conditions must not change significantly due to this height change. Sets of images were taken when the fluid level reached 3 cm, 5 cm, 7 cm and 9 cm at two different pulse separations, this was necessary due to the large difference in the velocity magnitude between the bulk fluid and the jet. The data from both pulse settings was then combined during analysis to give a complete picture of the velocity fields, an example MATLAB code is included in the appendix.

As a large amount of the mixing that occurs is laminar the areas of high shear in the vessel are important, as it is the elongation and shear as well as folding of fluid that causes it to mix. The magnitude of the shear rate in the x and y direction is calculated by:

$$\dot{\gamma} = \left|\frac{\partial v_x}{\partial y}\right| + \left|\frac{\partial v_y}{\partial x}\right| \qquad (3.7)$$

This is then plotted as a colour map with the velocity vector field, to show the regions of high shear.

Chapter 4 PLIF – Concentration fields[1]

4.1   Introduction

The results presented in this Chapter provide basic knowledge of the mixing in the simplified systems described in section 3.2. The first of these had the inlet pipe fixed 1 cm from the base of the tank; later experiments used a traverse to keep the pipe above the liquid free-surface as the vessel filled. Jets with nine different Reynolds numbers from 259 to 2867 were investigated by changing both the jet exit velocity and the viscosity of the fluid, this range allowed the transition from relatively unmixed laminar flows to better mixed turbulent flows to be observed and identified.

The technique employed in this Chapter to determine the mixing properties of the flow was Planar Laser Induced Fluorescence (PLIF) as described in section 3.4. The results obtained from this technique are discussed and where possible conclusions have been drawn.

4.2   Static pipe

4.2.1   Log Variance analysis

The simplest system set up investigated using PLIF had a fixed pipe inlet (as described in section 3.2) this system was used to develop the PLIF measurement technique over an appropriate range of flow conditions chosen for investigation; these conditions are described in Table 3.1.

---

[1] A selection of the PLIF results presented in this Chapter for the fixed pipe inlet have been published in the archival Journal Experiments in Fluids (Neal *et al.,*. 2008)

Figure 4.1 Evolving concentration fields at different fill heights for the 6 mPa s fluid at (a) h = 2.2 cm; (b) h = 4.7 cm; (c) h = 7.3 cm; (d) h = 10.3 cm at Re=661 (Q = 1.67 × 10^{-5} m^3 s^{-1}).
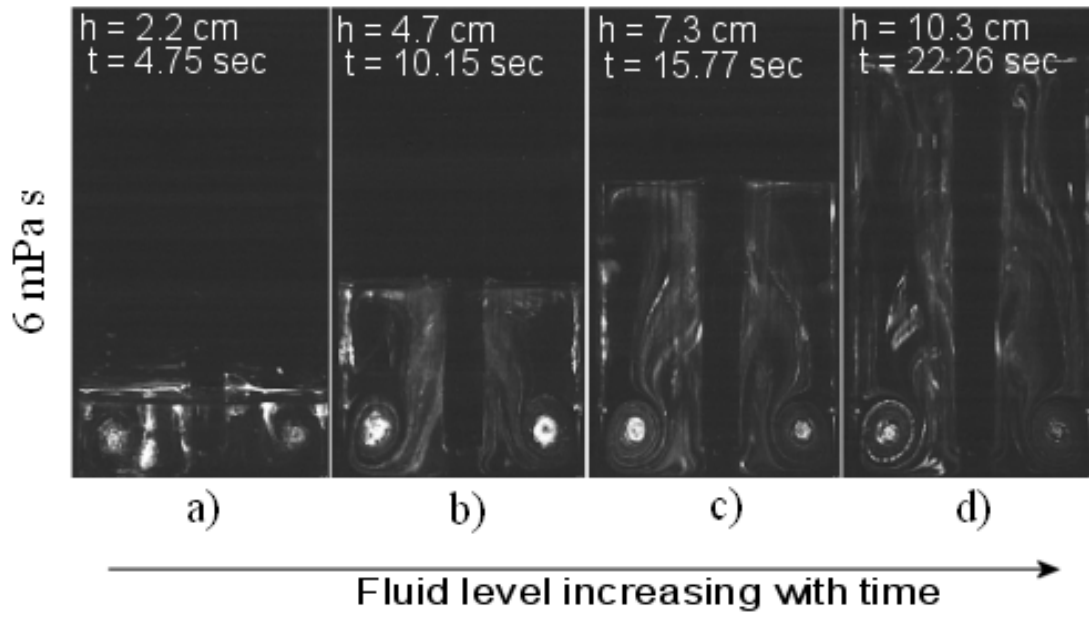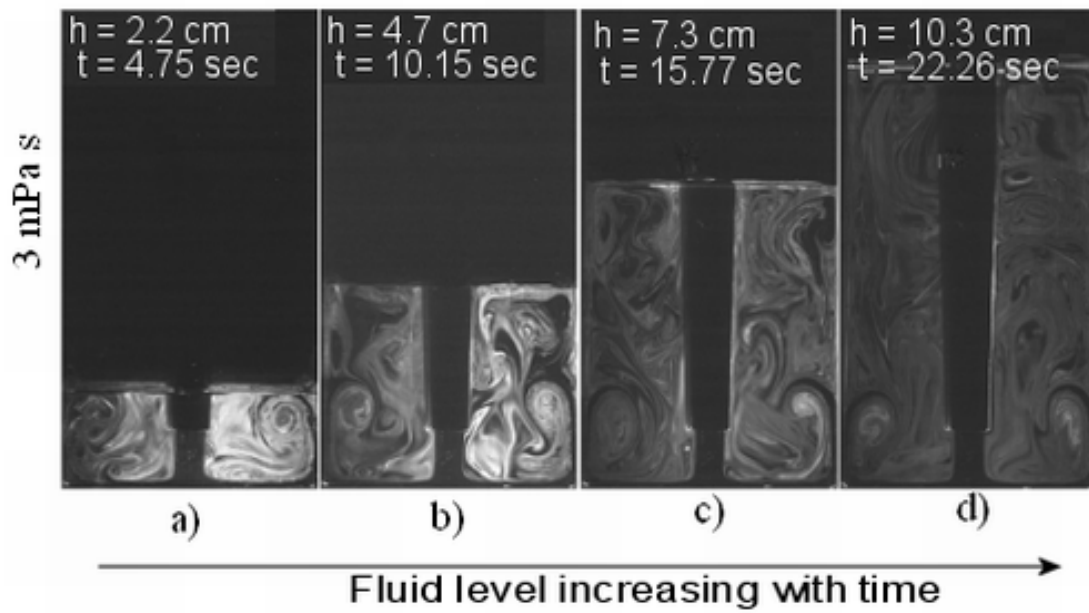

Figure 4.2 Evolving concentration fields at different fill heights for the 3 mPa s fluid at (a) h = 2.2 cm; (b) h = 4.7 cm; (c) h = 7.3 cm; (d) h = 10.3 cm at Re = 1245 (Q = 1.67 × 10^{-5} m^3 s^{-1}).

Figure 4.1 and Figure 4.2 show greyscale images taken by the CCD camera for the 6 and 3mPas fluids at values of Re of 661 and 1245 respectively. Both fluids generate a similar flow pattern; a toroidal vortex is formed in the bottom quarter of the vessel (Figure 4.1a, Figure 4.2a) whilst the flow in the upper half of the vessel is comparably quiescent and does not have a well defined structure (Figure 4.1c-d, Figure 4.2c-d). The striations created by the fluorescent tracer remain more defined in the low Reynolds number fluid than for the high Reynolds number fluid when the vessel is filled; although clearly in neither case is the vessel fully mixed.

Using the naked eye, the degree of mixedness appears to be higher for the higher Reynolds number fluid as both the scale of the striations is smaller and the contrast between them is lower, suggesting qualitatively a reduction in both the scale and intensity of segregation respectively. The existence of the striations throughout the filling process is indicative of a predominantly laminar mixing process (Ottino, 1989) since eddy diffusion would be expected to eliminate them if the flow were turbulent. The images shown here may form a basis for a mechanistic determination of the transition to turbulence, since, if molecular diffusion is considered negligible, a laminar mechanism would be characterised by clearly identified striations of black and white, whilst eddy diffusion would be expected to cause regions of 'grey'. Comparing Figure 4.1d and Figure 4.2d, regions of the vessel appear more mixed in Figure 4.2d, which is perhaps indicative of the beginning of this process.

Figure 4.3 Mixing performance for three different fluid viscosities at a fill rate of Q = 1.67× 10⁻⁵ m³ s⁻¹ (a) log variance plotted against dimensionless fluid height (H/T); Image of the vessel filled with fluid at (b) Re=343 (12 mPa s), (c) Re=661 (6 mPa s), (d) Re=1245 (3 mPa s).

Figure 4.3a shows the log-variance, as described in section 3.4.3, as a function of dimensionless fluid height (h/T) in the vessel for three fluids of decreasing viscosity at the same fill rate of $Q = 1.67 \times 10^{-5}$ m³s⁻¹, giving Reynolds numbers of 343, 661 and 1245 respectively. Each experiment was repeated a minimum of two times. At a value of *Re* of 1245 (red line), the log-variance reaches a minimum of ~ -1.8 (87% mixed) once the vessel is filled beyond 3 cm in height and remains constant until the

fill is complete. At values of *Re* of 661 and 343 (blue and green lines respectively), the log-variance stays at a value close to zero throughout the fill, indicating that the vessel remains unmixed.

There is a high level of noise in the log-variance plot, a small amount of which will be due to the measurement technique however comparison between the low and higher Reynolds number flows show that there is an increase in the noise for the higher Reynolds number, this could be caused by areas of high or low concentration moving through the measurement plane tangentially causing the average concentration in the measurement plane to fluctuate.

These results are borne out by the images shown in b-d which display an image of the filled vessel taken at the instant after completion of the filling process at values of *Re* of 343, 661 and 1245 respectively. The tracer remains unmixed with the bulk of the fluid in Figure 4.3b and c and is located either in the toroidal vortices at the bottom of the vessel or is swept up close to the fill pipe or the free surface. At *Re* = 1245, as shown in Figure 4.3d, the mixing performance is much improved and the tracer is spread over the entirety of the vessel, although striations of black, where no tracer is present, are still visible. Comparison of the visual images with the log-variance analysis is most revealing; although the log-variance analysis can be used to determine that the vessels are in an unmixed state, at *Re* = 1245, the degree of information on the level of mixedness shown in the image is much higher than can be represented by a single parameter such as log-variance. The results are also remarkable in that a threefold increase in fluid viscosity causes the vessel to go from a relatively well mixed state to almost unmixed at the same flow conditions.
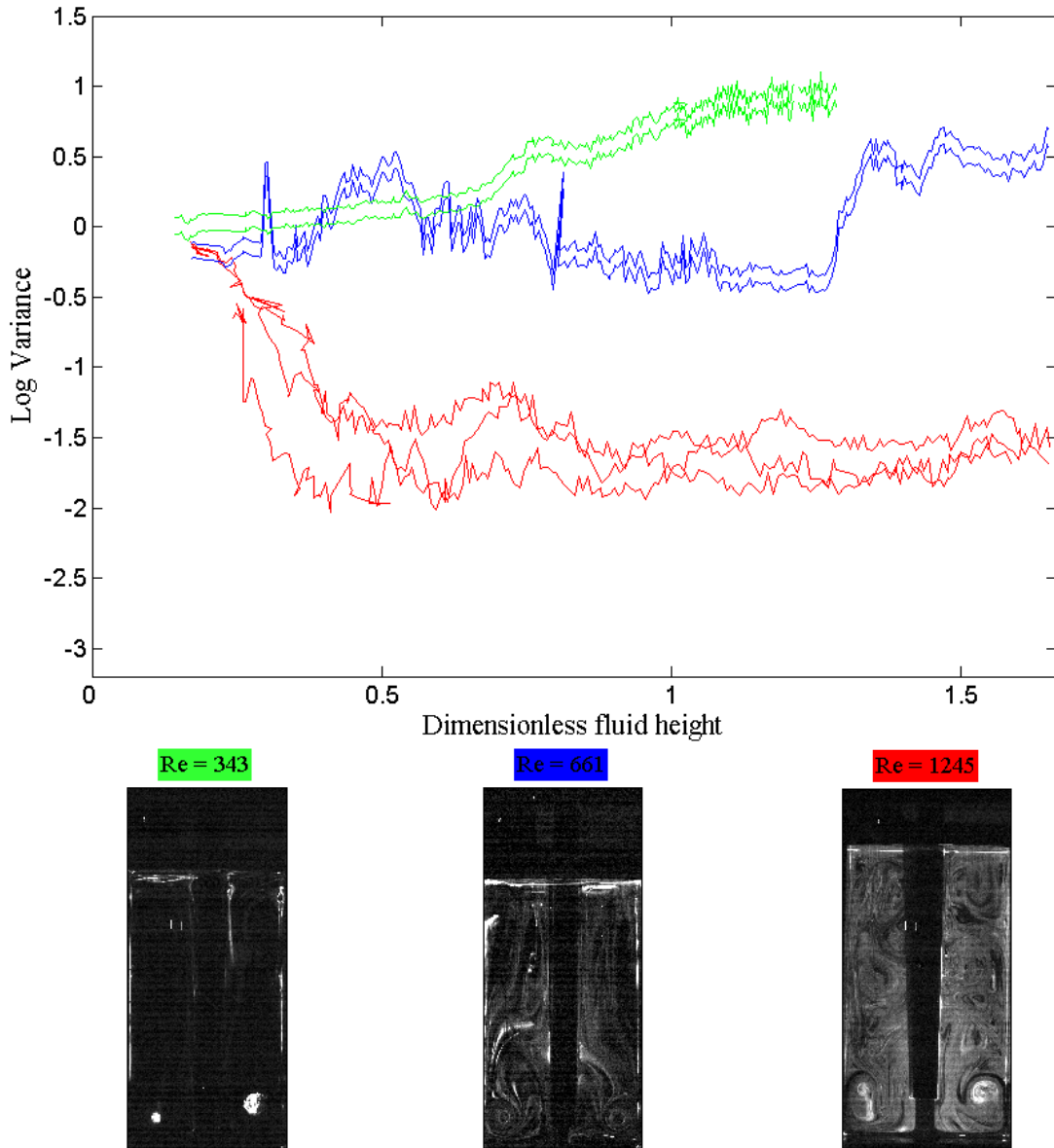
Figure 4.4 Mixing performance for three different fluid viscosities at a fill rate of $Q = 3.33 \times 10^{-5} \, m^3 \, s^{-1}$ (a) log variance plotted against dimensionless fluid height (H/T); Image of the vessel filled with fluid at (b) Re=687 (12 mPa s), (c) Re=1322 (6 mPa s), (d) Re=2490 (3 mPa s).

Figure 4.4 shows similar data for fluids with the same three decreasing viscosities at a higher fill rate, Q of 3.33×10^{-5} m^{3}s^{-1}, giving values of *Re* of 687, 1322 and 2490 respectively. Again, at the lowest value of *Re* (687), the log-variance remains close to zero (Figure 4.4a) and the tracer remains unmixed through the bulk of the vessel

(Figure 4.4b). The mixing performance at the higher values of Re of 1322 and 2490 improves noticeably, with the log variance reaching ~ -1.5 (82% mixed) and -2.5 (94% mixed) respectively. Notably, for the experiment with the value of Re equal to 1322 (6 mPa s fluid, Figure 4.4c), the degree of mixedness is qualitatively similar to the experiment obtained at $Re = 1245$ (3 mPa s fluid, Figure 4.3d); it would be expected that Re would be an important part of any scaling criterion. At $Re = 2490$, the tracer appears visually to be almost uniformly mixed through the vessel and very few striations are present; this may be indicative of a change of mixing mechanism from laminar to turbulent.

The change in mixing mechanism is even more apparent at the highest flow rate used, $Q = 5 \times 10^{-5}$ m^{3}s^{-1}. The change in flow is still not sufficient to mix the highest viscosity fluid at $Re = 1030$, (Figure 4.5b) but for $Re = 1983$ and $Re = 3735$ the distribution of the tracer in the tank (Figure 4.5c,d respectively) is almost uniform. The log-variance drops to -2.2 (92% mixed) and -3 (97% mixed) for the lower viscosity fluids at $Re = 1983$ and $Re = 3735$ respectively when the dimensionless fill height (h/T) is of the order 0.5-1. However, upon further filling of the vessel, the mixing performance actually worsens and the log-variance begins to rise again, reaching – 1.8 at $Re = 1983$ (87% mixed) and -2.4 (94% mixed) at $Re = 3735$. The worsening in mixing performance can be attributed to the quiescent nature of the flow in the top half of the vessel and to the linear drop in specific energy input as the vessel is filled.

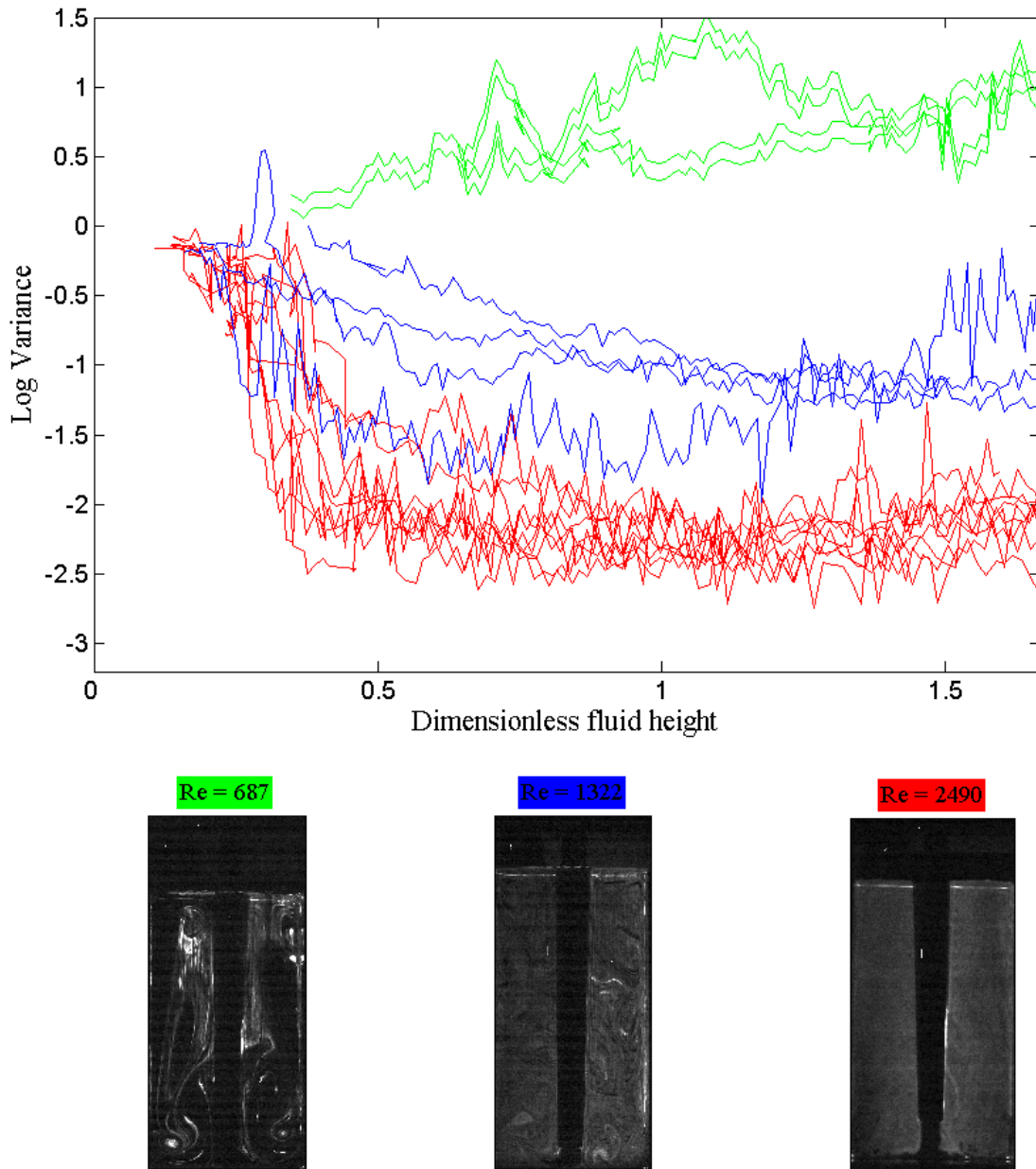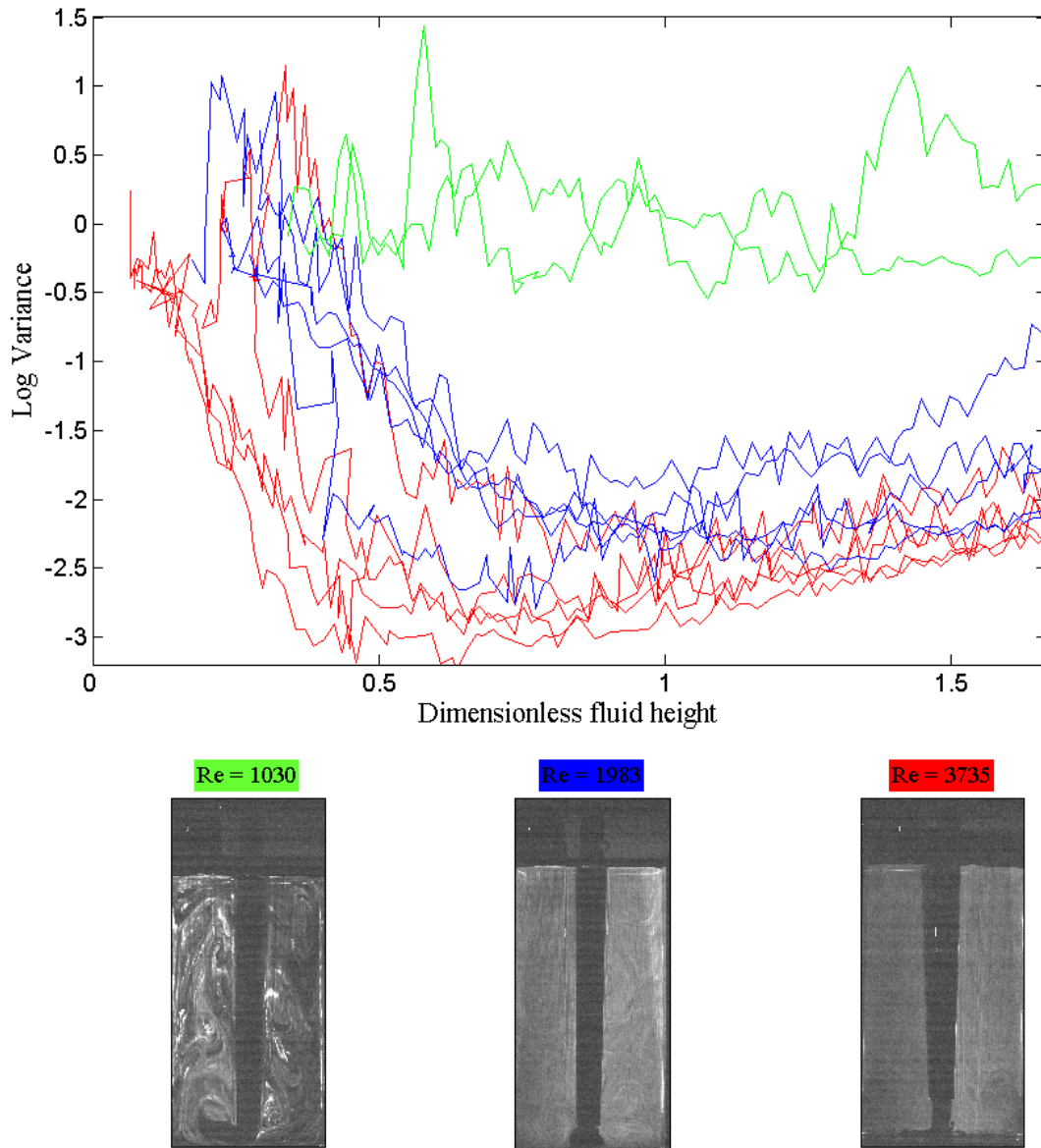*Figure 4.5 Mixing performance for three different fluid viscosities at a fill rate of $Q = 5.00 \times 10^{-5}$ m^3 s^{-1} (a) log variance plotted against dimensionless fluid height (H/T); Image of the vessel filled with fluid at (b) Re=1030 (12 mPa s), (c) Re=1983 (6 mPa s), (d) Re=3735 (3 mPa s).*

For flows that appear to be dominated by laminar mixing, the toroidal vortices are visible, Figure 4.6 and Figure 4.7 show the position of this vortex in relation to the base of the tank and the inlet pipe at values of *Re* of 343, 661 and 1245 respectively ($Q = 1.67 \times 10^{-5}$ $m^3 s^{-1}$). It can be seen from Figure 4.6 that as the viscosity increases the vortex centre moves closer to the base of the tank. For all three viscosities the

height of the vortex at the beginning of the fill is less than 50% of the fluid height, perhaps caused by interactions with the free surface of the fluid. As the fluid height increases so does the vortex height until it reaches a maximum value which increases with *Re*. At *Re* = 343, the vortex height that does not fluctuate significantly from its maximum. However as the viscosity decreases there appears to be more instability in the vortex position; this instability is also evident in Figure 4.7. At *Re* = 1245, the fluctuations have a standard deviation of 8%, this may be the first signs of a more turbulent flow regime.
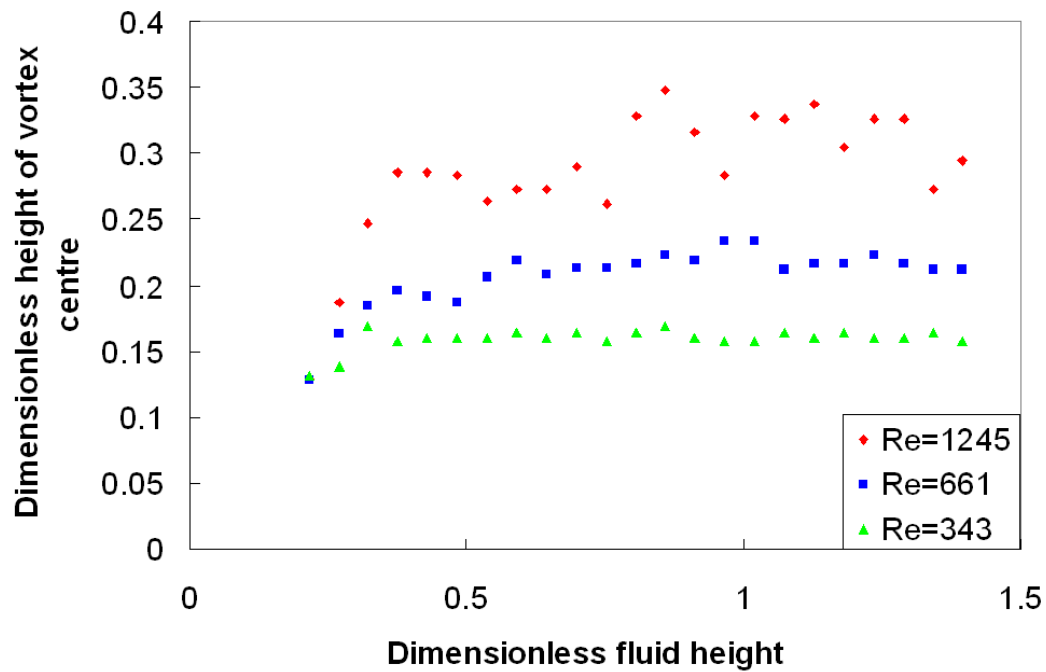
Figure 4.6 The dimensionless height (h/T) of the centre of the vortex from the base of the tank, measured for three Reynolds numbers at flow rate of Q = 1.67 × 10^{-5} m^3 s^{-1}

Figure 4.7 shows that the average horizontal distance of the vortex from the pipe does not vary significantly across the values of *Re* used in these experiments which suggests that it is affected only by the geometry. This implies that the vortices are the same size for the different viscosities but they have just moved further up the vessel.

While this is true for the higher two viscosities which are still within the laminar flow regime, the 3 mPa s fluid shows a large amount of distortion of the vortex which could again be evidence of the beginning of turbulent fluctuations. It may prove possible to exploit these vortices to further improve the mixing performance by manipulating the geometry: clearly this will also alter the ratio of the jet to tank Reynolds numbers and the distribution of local specific energy dissipation rate.
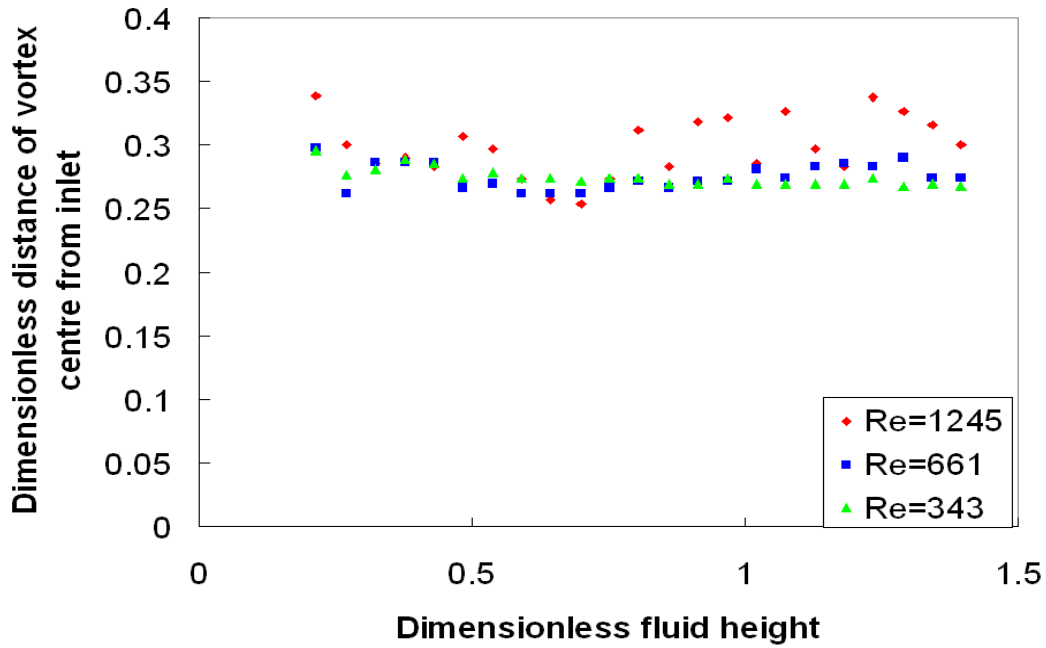
Figure 4.7   The dimensionless horizontal distance of the centre (h/T) of the vortex from the edge of the inlet pipe, measured for three Reynolds numbers at flow rate of Q = 1.67× 10^{-5} m^3 s^{-1}

4.2.2   Flow regime in the vessel

The transition between laminar and turbulent flow is normally defined on the basis of a critical value of *Re* determined experimentally for a given system. This value can vary substantially, since the choice of length and velocity scales depends on the geometry in question.. As shown in section 3.3.1, the values of *Re* based upon the dip

pipe diameter and jet exit velocity are of $O(10^3)$. An alternative would be to consider a tank Reynolds number based upon the flow in the vessel, using the tank width and the superficial velocity of the fluid (based on the cross-sectional area of the tank bottom) as the length and velocity scales respectively. This would give Reynolds numbers of $O(10)$. Clearly, for the constant geometry used in these experiments, the ratio of the jet and tank Reynolds numbers is also constant.

However, it is not sufficient to use Re as the sole parameter to characterize the mixing performance. In the characterization of mixing in stirred vessels of constant volume, a critical parameter is the energy input per unit mass, ε, which can be evaluated locally and also averaged over the whole vessel. Indeed Kresta & Wood (1993) stated that prediction of the local specific energy dissipation rate, ε_T, is, in many cases, the key to successful process modeling. In the filling case, the analysis is complicated since the mass of liquid in the vessel increases linearly in time. At the start of the filling process, when the mass in the tank is small, the energy input per unit mass is high which causes intense mixing. As shown in Figure 4.1a and Figure 4.2a, the initial charge of tracer is swept off the bottom of the vessel and the initial mixing performance is commensurate with the high specific energy of the fluid. As the vessel is filled further, the energy input per unit mass drops linearly with time and the mixing performance noticeably worsens: Figure 4.1 and Figure 4.2 (b-d) demonstrate that the tracer is swept upwards near the dip tube as it exits the toroidal vortex and does not appreciably mix further with the fresh fluid entering the vessel. This effect is more noticeable with the higher viscosity fluid, which is to be expected since the value of Re is half that of the lower viscosity fluid. The extra mixing of the low viscosity fluid may be either due to the creation of eddies via turbulence or due to

molecular diffusion. Assuming the Stokes-Einstein relationship between viscosity and molecular diffusivity holds ($\mu \sim D_M^{-1}$); mixing due to molecular diffusion would be twice as rapid in the low viscosity fluid. If one were to consider the remainder of the mixing process being completed by this mechanism, assuming that $D_M = O(10^{-8})$ m^2s^{-1}, then if the striations were 10% of the vessel diameter, the diffusion time,

$$t_d = \frac{\lambda^2}{D_M} = \frac{(0.1T)^2}{D_M}$$

This gives $t_D \sim 3600$ s for $T = 0.06$ m, or about one hour. This would be possible for single phase bottled products during shipping. Over a fill time of ~ 20 s, assuming the same value of D_M, molecular diffusion would only occur over a length-scale of ~ 500 μm, an almost negligible amount.

4.3   Moving pipe

Figure 4.8 shows the log variance as a function of fluid height for three Reynolds numbers using the moving pipe described in section 3.2.2; the mixing improves as the Reynolds number increases as in the fixed pipe experiments. The lowest Re = 257 shows very little mixing throughout the fill with the log variance staying around zero, this is comparable to the static pipe results at similar Reynolds numbers where the mixing does not improve throughout the fill. For the highest Reynolds number Re = 2867 the log variance decreases to $\sim$ -2.6 indicating that it has reached 95% mixed. Between these two is the Re = 996 case where some mixing occurs but not sufficient to reach the 95% level, here the log variance reaches $\sim$ -1.5. For both cases where mixing occurs once the fill height has reached 5 - 6 cm, there is little further improvement to the mixedness and in some cases the log variance increases indicating

55

that the 'fresh' fluid entering the vessel is no longer mixing as effectively. For the

highest Reynolds number this may be due to the fact that there is always an area of

lower tracer concentration around the jet, so despite the homogeneity in the

surrounding liquid the variance cannot be decreased further.
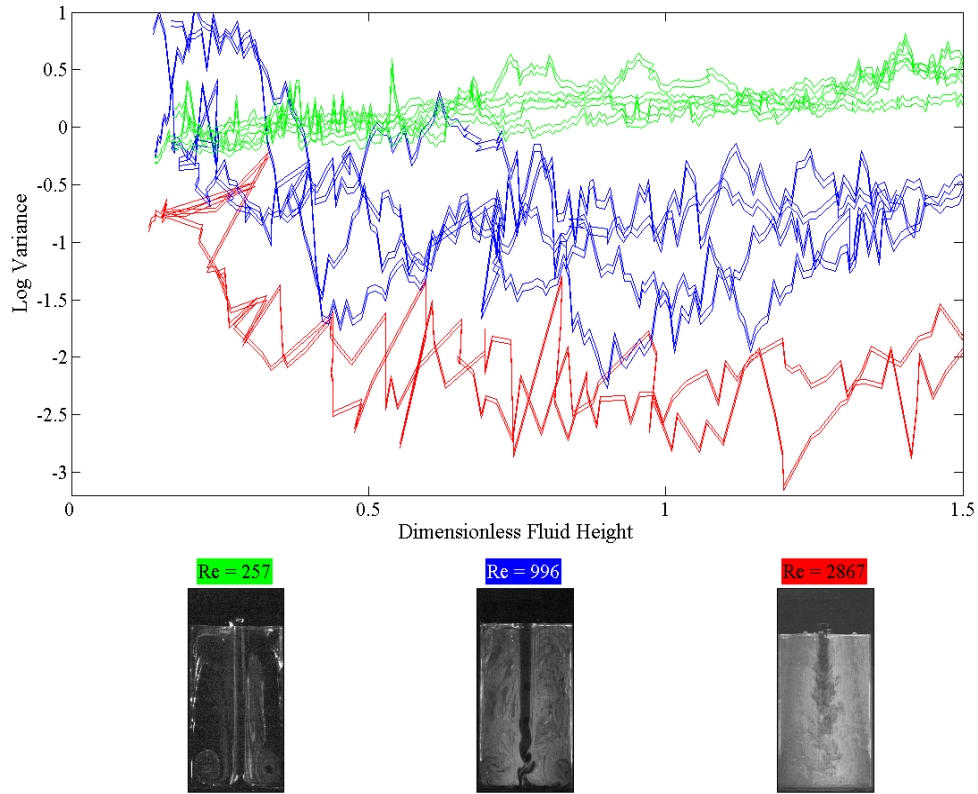
Figure 4.8   Mixing performance for three different fluid viscosities at a fill rate of Q = 5.00×10⁻⁵ m³ s⁻

^{1} *(a) log variance plotted against fluid height; Image of the vessel filled with the (b) 16 mPa s fluid, (c)*

8 mPa s fluid, (d) 4 mPa s fluid

Figure 4.8b-d show a very clear change in the mixing mechanism, the Re = 257 fluid

(Figure 4.8b), the tracer is distributed around the vessel but there are two toroidal

vortices and obvious striations which indicate laminar flow conditions. The highest

Reynolds number fluid *Re* = 2867 (Figure 4.8d), is a more turbulent flow and as a

result it shows a more uniform distribution of dye, the striations have been removed

through eddy diffusion. For the *Re* = 996 (Figure 4.8c) case there are still striations

visible but there is more uniformity than the *Re* = 257 case, this shows the transition between the two different flow regimes. This agrees with the fixed pipe case described in section 4.2.1 where the transition occurred around *Re*~1000.

A further indication of the onset of turbulence is the stability of the jet, the more laminar jet (Figure 4.8b) shows the 'fresh fluid' travelling directly to the base of the tank without undergoing spreading or jet break up and hence little mixing. The transition jet shows similar travel to the base of the tank of the fresh fluid, however as the jet becomes longer with the surface rising instabilities appear towards the base (Figure 4.8c) indictating the jet is no longer purely laminar. The turbulent jet (Figure 4.8d) shows the jet mixing quickly with the surrounding fluid due to the jet spreading and eddies forming.

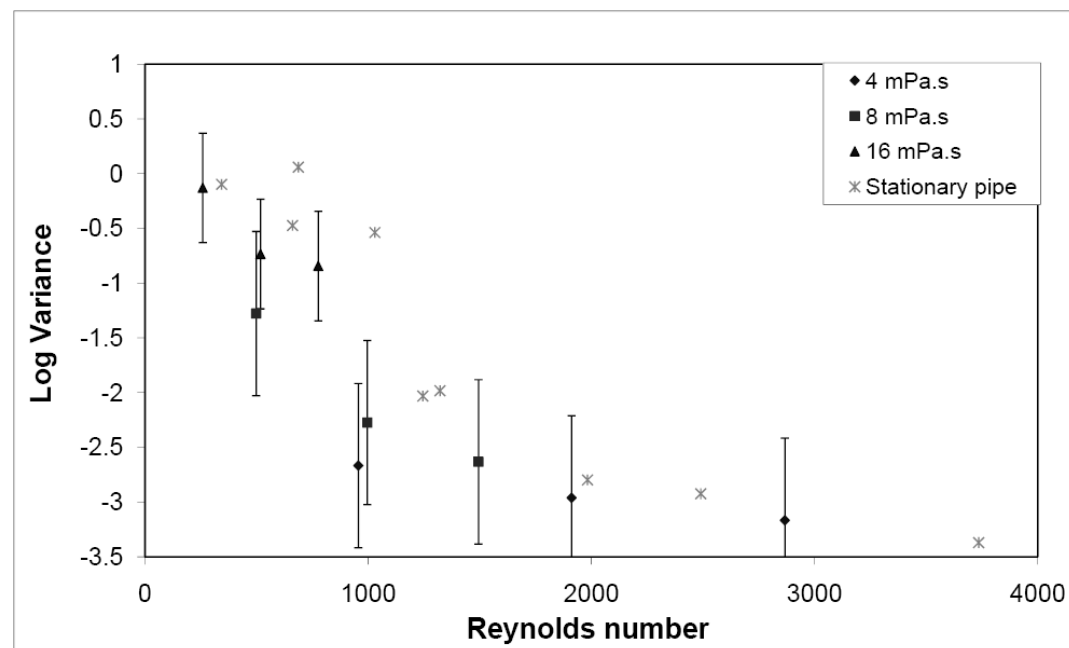### 4.3.1   Mixing performance and mixing mechanism.

Figure 4.9 Plot of the minimum log variance reached in each experiment versus the jet Reynolds number.

Figure *4.9* shows the minimum log variance reached by each experiment compared with the Reynolds number of the jet in each case. The log variance in the tank decreases rapidly as the Reynolds number increases for small values of *Re*. However once the log variance decreases to below -2.5 this improvement in mixing becomes more gradual, this occurs for Reynolds numbers above 1000. The mixing mechanisms appear from the images to be a combination of laminar and turbulent, with the turbulent mechanism becoming dominant above a value of *Re* of ~1000, the evidence for this being the disappearance of the toroidal vortices and the appearance of instabilities in the jet. This agrees with Kim *et al.* (2007) who observed the stability of a water jet and found it was steady at *Re* = 404 but had become unsteady when it reached *Re* = 1026.

In comparison with the stationary pipe results (Figure *4.9*) using a moving pipe appears to improve the mixing performance at the same liquid flow rate. From observing the images the flow appears to be more turbulent with the moving pipe, possibly because of the increasing length of the free jet which allowed instabilities to develop. Also mixing will also have been improved by increasing entrainment into the jet from the top half of the vessel.

It should be noted that the level of mixing in the tank has not reached the limit of the resolution of the camera. For very highly mixed conditions the ability of this technique to measure the fluctuations in concentration will be limited by the pixel size in the captured image.

4.3.2 Obstructed jet.

Figure 4.10 shows the flow pattern at different points in the fill for the Re = 1494 fluid, this clearly shows the striations that form in the tank and the improvement in the mixing as the jet length increases. However a small number of nominally identical experiments showed a different flow pattern, as shown in Figure 4.11a visual comparison between Figure 4.10 and Figure 4.11 shows that the tank in Figure 4.11 appears to be better mixed, this is verified by comparing the log variance of the two which is shown in Figure 4.12.
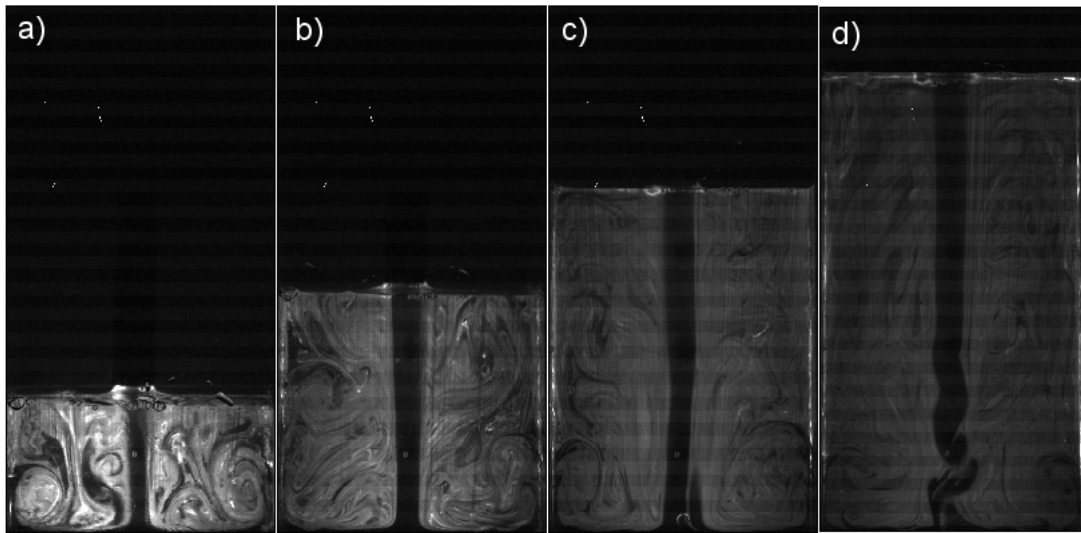
Figure 4.10 Evolving concentration fields at different fill heights for an 8 mPa s fluid, Re=1494 at (a) h = 2.2 cm; (b) h = 4.7 cm; (c) h = 7.3 cm; (d) h = 10.3 cm at a flow rate Q = 3.33 × 10^{-5} m^3 s^{-1} through a 6 mm dip pipe.
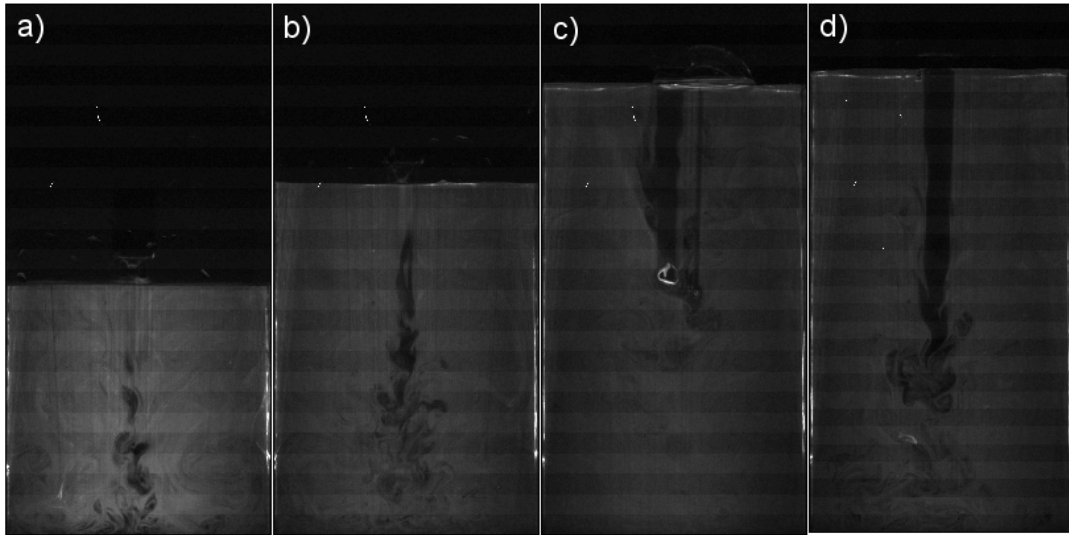
Figure 4.11   Evolving concentration fields at different fill heights for an 8 mPa s fluid, Re=1494 where a bubble has formed at (a) h = 2.2 cm; (b) h = 4.7 cm; (c) h = 7.3 cm; (d) h = 10.3 cm at a flow rate Q = 3.33 × 10^{-5} m^3 s^{-1} through a 6 mm dip pipe.

Unlike Figure 4.10, in Figure 4.11a-b the dark jet is not clearly visible down the centre of the tank although small areas of low concentration can be seen towards the base, this suggests that the jet has been obstructed in some way and the fluid is now entering the tank away from the centre plane. Figure 4.11c shows a bubble being released into the flow, behind which the jet becomes clearly visible; in Figure 4.11d the jet is now flowing through the centre of the tank. It appears that this bubble was obstructing the jet, the dark eddies seen towards the base in Figure 4.11a-b suggest that this obstruction has made the jet instable fortuitously creating a more turbulent flow and better mixing. This mixing improvement could be created in the process by putting a permanent obstruction in the end of the dip pipe, this is investigated in Section 6.3. However, not surprisingly, the random presence of the bubble led to unreliable reproduction of the result in Figure 4.11.
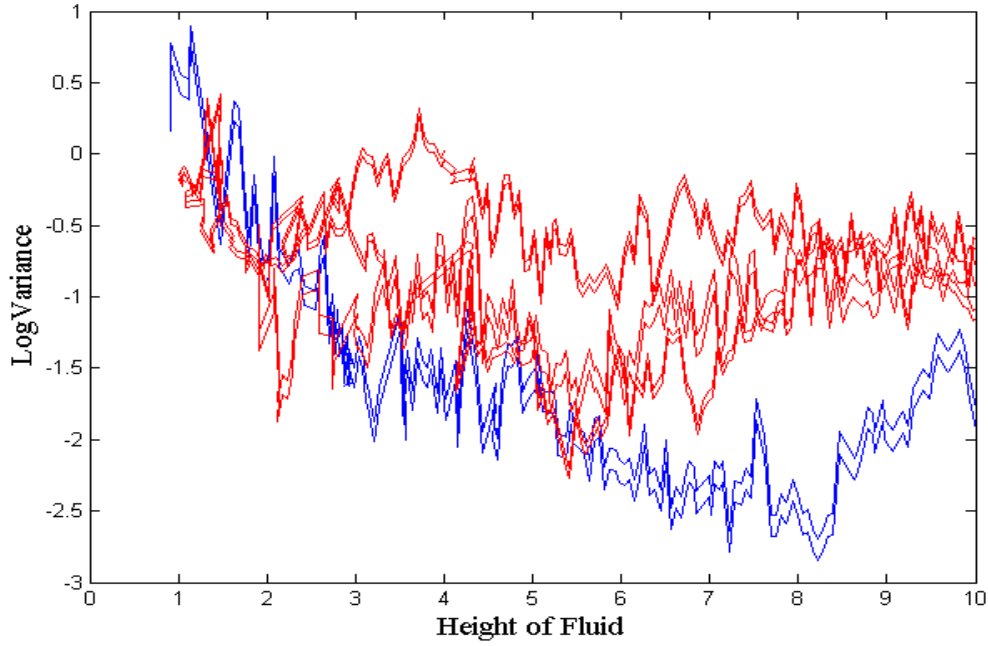
Figure 4.12 The log variance plot of two fills of the 8 mPa s fluid at a flow rate Q = 3.33 × × 10^{-5} m^3 s^{-} where a bubble has formed under the pipe in one (blue) and the jet is unobstructed in the other (red)

4.4   Conclusions

The PLIF technique has been demonstrated to give good repeatability for the same flow conditions and qualitative examination of the images has revealed a change in the mixing mechanism from laminar to turbulent above a critical value of the Reynolds number (*Re*~1000) which agrees with previous literature. For the cases above *Re*~1000 the log variance reaches -2 which equates to 90% mixed. The use of a retracting inlet pipe is shown to give a small increase in the mixing performance, above *Re*~1000 the log variance reaches -2.2 in each case which equates to 92% mixed. The retracting pipe also allows the stability of the jet to be examined giving further evidence of the mixing regime in the tank. A bubble causing an obstruction in the end of the pipe improved the mixing performance and could be replicated in the nozzle design to provide this improvement in a more reliable way.

Chapter 5 Velocity Fields

5.1 Introduction

To gain a better understanding of the mechanisms effecting the mixing in the tank the velocity distribution was investigated using PIV. A comparison between the flow patterns in the cases where the jet was able to mix the fluid and those where the mixing was unsuccessful was made. In these cases the dead regions in the tank could be identified and the areas where the shear rates are higher and more mixing occurred highlighted. This chapter looks at the velocity profile and structure in the jet, a comparison between jets at different Reynolds numbers is then made. The links between the mixing in the tank and the flow patterns are made.

The PIV was set up as described in section 3.5, this allowed the flow field in the vessel to be measured for the same values of Reynolds numbers as for the PLIF results, these conditions are shown in Table 3.1

5.2 Velocity profiles

The general structure of the jet impinging on a pool of liquid is shown in Figure 5.1; this jet structure in this region agrees with previous works as described by Reungoat *et al.* (2007). The fluid enters the tank at the top of the vessel and travels vertically downwards until it reaches the impingement zone, it is then forced along the base of the tank towards the walls, at this point the fluid has lost the majority of its momentum and the subsequent upwards movement is slow. This slow upward

velocity is directed slightly towards the jet as it replaces the fluid that has been entrained as well as fuelling the rising free surface.
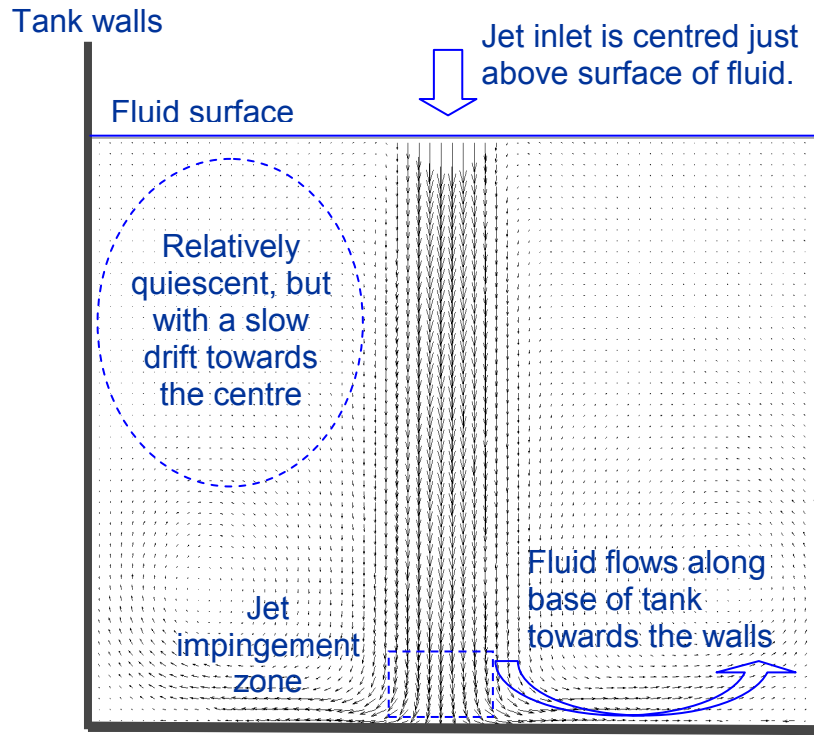
Figure 5.1   An example of the PIV velocity profile in a vessel showing the features present in all cases.
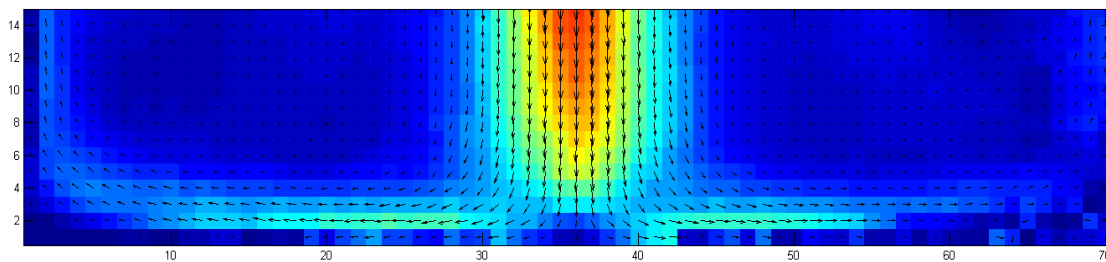
Figure 5.2   Jet impingement zone, shaded to indicate velocity magnitude

Figure 5.2. shows the jet impingement zone at the base of the tank, the stagnation region in the centre of the jet is clearly visible however the low accuracy of the results next to the glass base means that the flow in the boundary layer cannot be analysed further. Dead zones can be seen in both the bottom corners of the tank where the

velocity is low caused by the abrupt change in direction of the jet along from the base to moving up the wall.
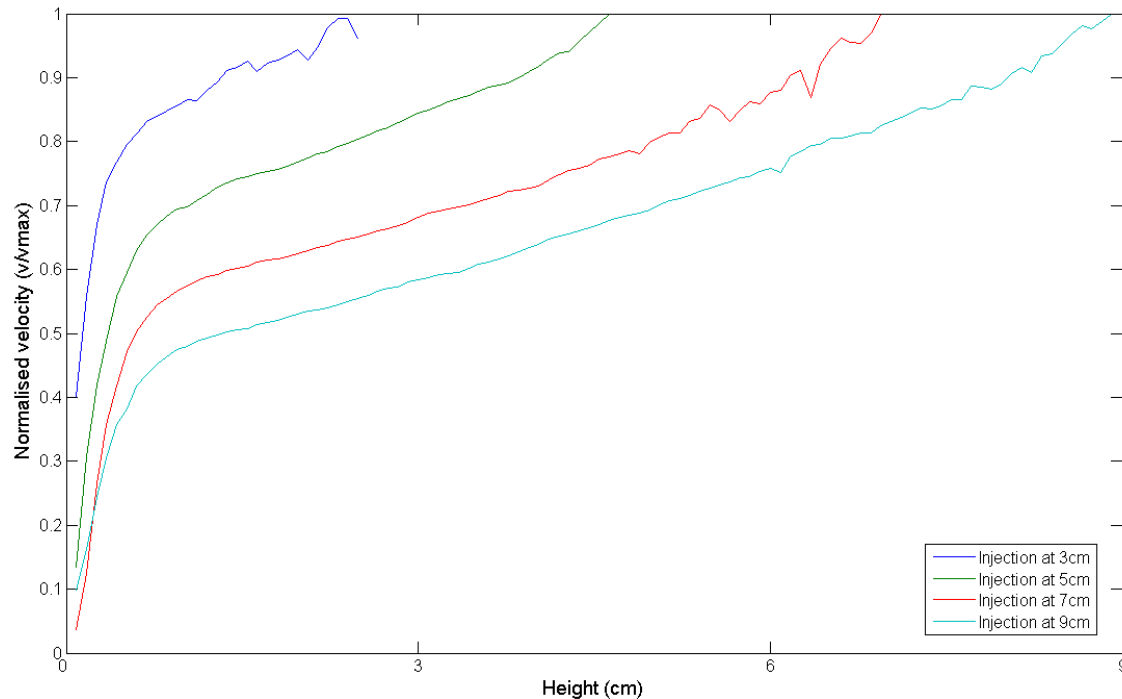
Figure 5.3. The change in normalised velocity along the jet centreline for the four different points in the fill

Further insight into the dynamics of the jet can be gained from Figs. 5.3 and 5.4. Figs 5.3 shows the decrease in the centreline velocity of the jet as it moves from the point of injection towards the point of impingement. The velocity has been normalised by dividing though by peak velocity at the end of the pipe to allow comparison. The deceleration of the jet is caused by the viscous drag of the surrounding fluid, this viscous drag causes energy to be dissipated and also the surrounding fluid to become entrained into the jet, the more the surrounding fluid is entrained the more kinetic energy is transferred to the rest of the tank. The deceleration of the jet is relatively high near the point of injection and decreases to a

steady rate when the normalised velocity reaches ~ 0.8. The effect of the

impingement can be seen when the fluid reaches approximately 1 cm from the base

where the velocity suddenly begins to decrease more rapidly, this point is this same

regardless of how high the injection point is.
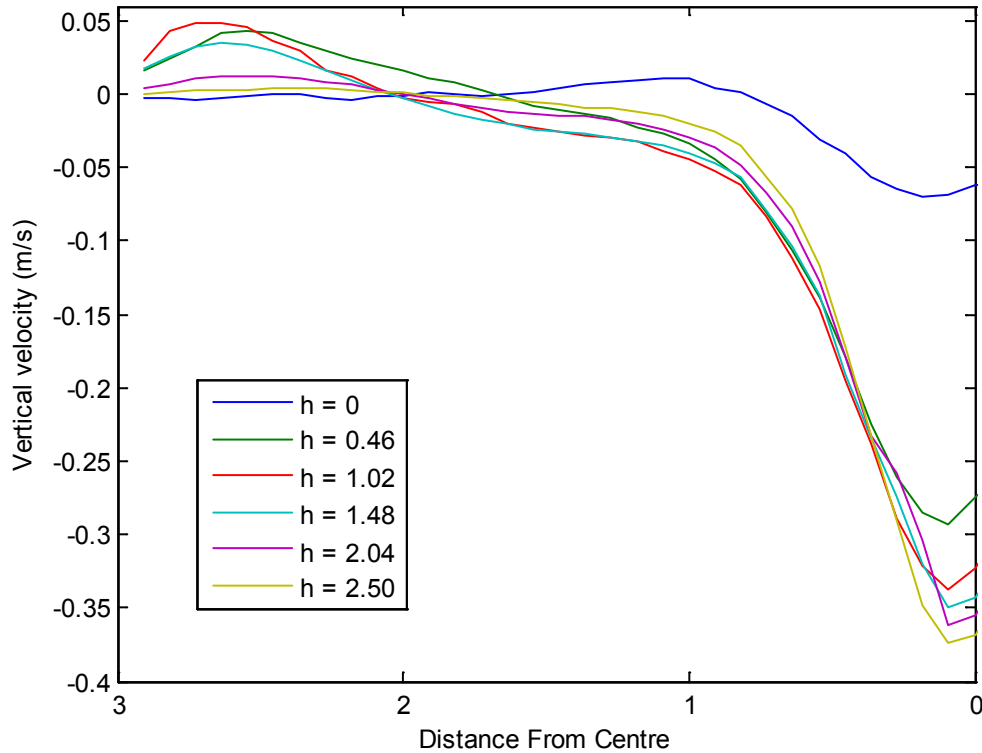
Figure 5.4. Vertical velocity profile across horizontal slices taken at heights h above the base of the tank

Figure 5.4. shows the velocity at points away from the centreline for the heights in

and near the impingement zone. At 2.5 cm the peak has well defined edges, moving

closer to the wall the peak spreads and there is a larger amount of upward velocity

towards the tank wall. For the data closest to the tank base this upward motion next to

the wall is not present, this is due to the dead zones in the corners of the tank
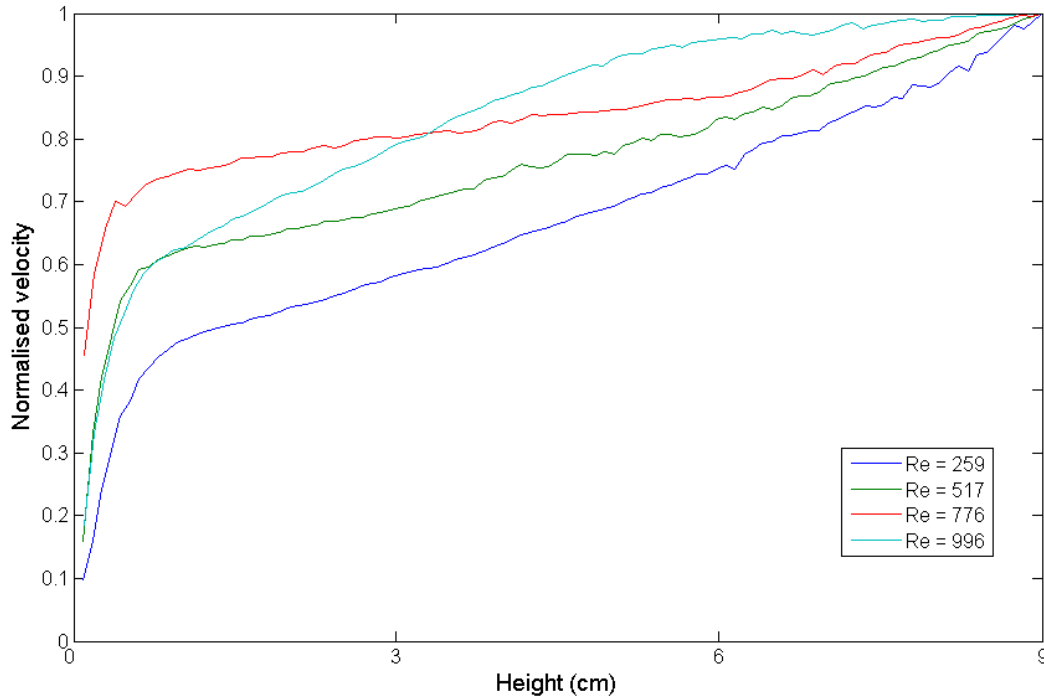
Figure 5.5. The centreline velocity profile for low Reynolds number fills when the injection height has reached 9 cm

Figure 5.5 shows the centreline velocity of the lower Reynolds number jets where the flow is mostly laminar, Figure 5.6 shows the same plot for the higher Reynolds numbers where flow appeared more turbulent, Re=959 appears in both graphs. For the laminar flows there is a change in the gradient of the jet velocity is as the Reynolds number is increased; the lower Reynolds numbers show the largest drop in the velocity along the jet. As the fluid is more viscous the drag on the edges of the fluid flow is larger and so the jet's kinetic energy is lost. At high Reynolds numbers the jet is turbulent, Figure 5.6 shows that once the transition to turbulence has occurred the gradient of the velocity decrease is approximately constant for all values of Reynolds number. The case with *Re*=996 does not fit into either catagory but is in transition between the two, this agrees with previous observations from the PLIF data of the onset of turbulence around this Reynolds number.
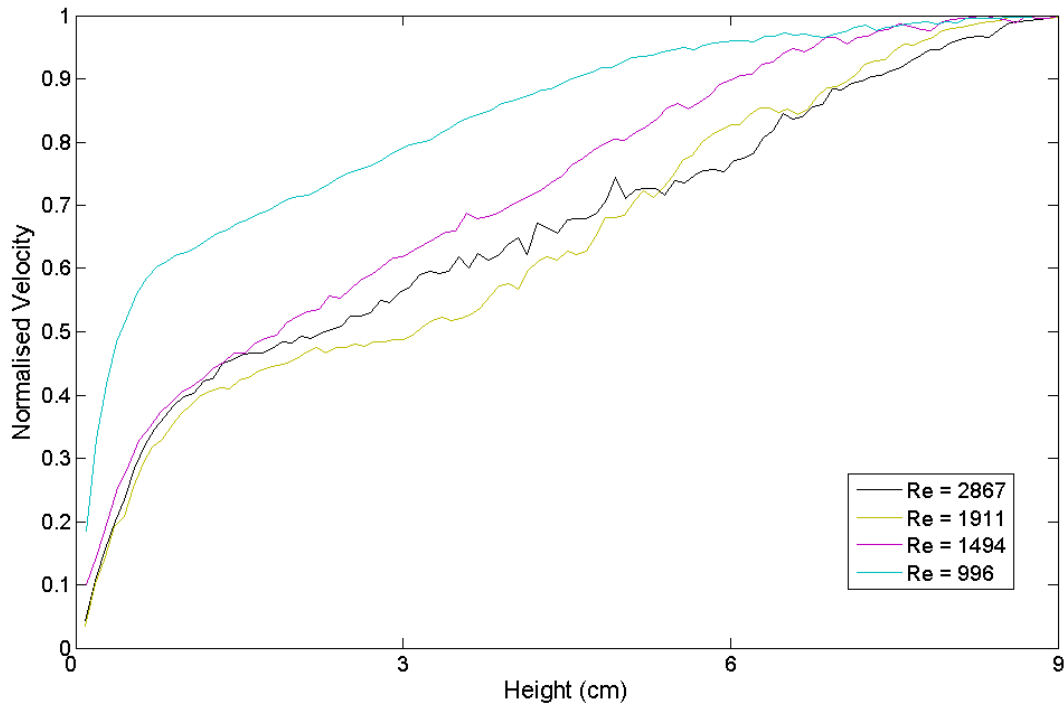
Figure 5.6. The centreline velocity profile for high Reynolds number fills when the injection height has reached 9 cm

The transition in the flow can be seen from the velocity magnitude plots (fig 5.7). For low Re there is very little observable detail of the velocity change in the top half of the vessel and the contours are fairly well defined; this flow showed the dye trapped along the wall or up the side of the vessel in the PLIF data. For the transitional flow there is some movement in the top of the vessel and the contours loose their smoothness, this flow exhibited the definite striations in the PLIF data. For the higher Re plots there is a larger amount of velocity fluctuation across the top of the tank, as this becomes more pronounced the corresponding PLIF data shows the jet becoming more unsteady and the mixing performance is improved. There is an error around the jet injection points caused by the moving pipe.
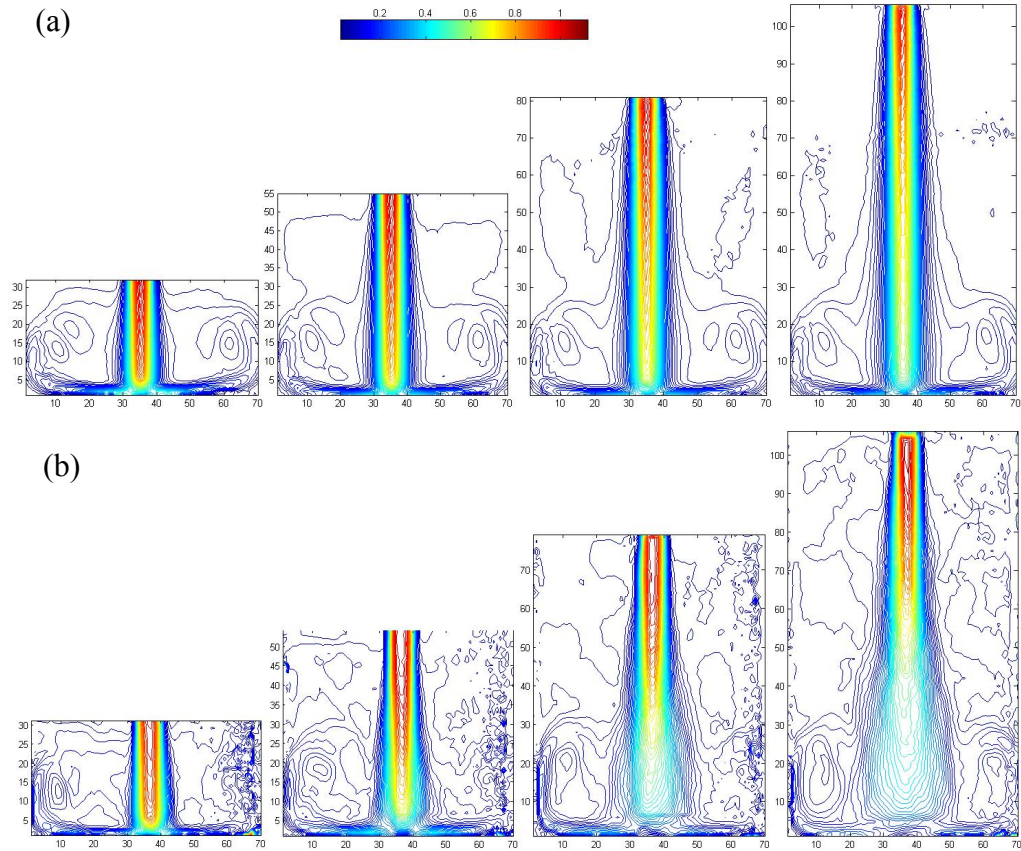
Figure 5.7. Velocity magnitude contour plots for flow at a) Re=517 and b) Re=1911

5.3   Shear rates

As a large amount of the mixing that occurs is laminar the areas of high shear in the vessel are important, as it is the elongation and shear as well as folding of fluid that causes it to mix. The magnitude of the shear rate in the following plots is calculated using equation 3.6.

 From Figure 5.8 it can be seen that the values of the shear are highest at the outsides of the jet, where there is a sharp change in the velocity and along the base of the tank where the jet moves radially away from the centre of the tank. These areas are where

the striations seen in the laminar flow originate; this is then folded by the recirculation in the tank.
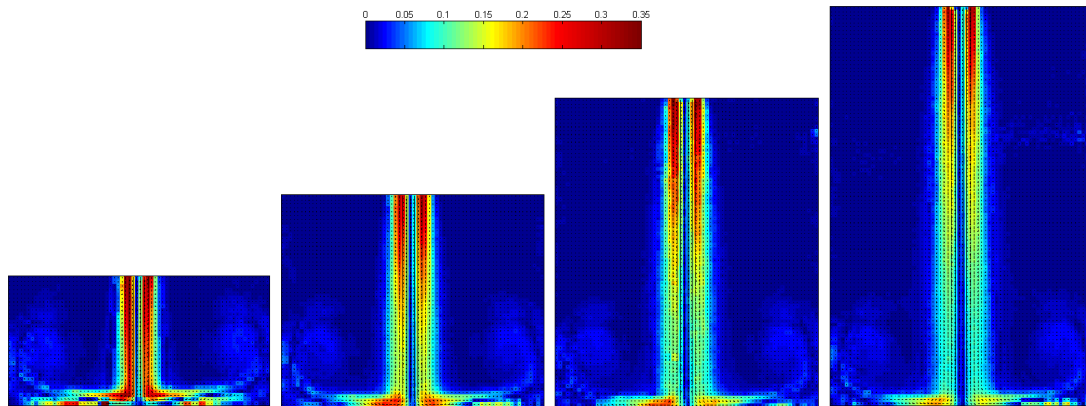
Figure 5.8. The shear rate calculated from the velocity field measured at Re=517

5.4   Conclusions

To examine the flow regime in the tank further PIV was used; the resulting vector fields allowed the distribution of momentum and shear in the tank to be investigated. For all flows, dead regions were observed in the bottom corners of the tank and the top half of the tank was relatively quiescent, however this was more prominent for more laminar flows. For the more turbulent flows (Re > 1000) there was a higher level of movement in the top half of the tank which corresponds to the increase in the mixing performance shown in Chapter 4. To improve the mixing performance in the laminar cases this movement must be created and accentuated by changing parameters such as tank or nozzle geometry.

Chapter 6 Flow improvements

6.1   Introduction

To improve the level of mixing in the tank for lower Reynolds number it is necessary to alter the flow patterns so that there is more energy being discipated in the top half of the tank. There are several ways in which this can be achieved, two different methods have been investigated, varying the flow rate of the jet and changing the design of the inlet nozzle. Section 6.2 examines the improvements due to ramping the flow rate or of applying a sinusoidal variation to the flow rate. Section 6.3 describes the increased level of mixing caused by changing the nozzle design.

6.2   Variable flow rate

As the tank is filled the energy from the jet dissipated per unit volume in the vessel decreases. This means that the level of mixing in the tank is greater at the start of the filling process than at the end, an effect that was demonstrated in Chapter 4. To prevent this drop off in the mixing performance the flow rate of the jet could be increased throughout the filling process. A case with this ramped flow was set up as described in section 3.2.3.

An alternative way of improving the mixing is to increase the perturbations in the top half of the jet, this has been achieved by varying the flow rate as a sinusoidal, this case was designed to provide fluctuations in the flow field that would increase the levels of turbulence.
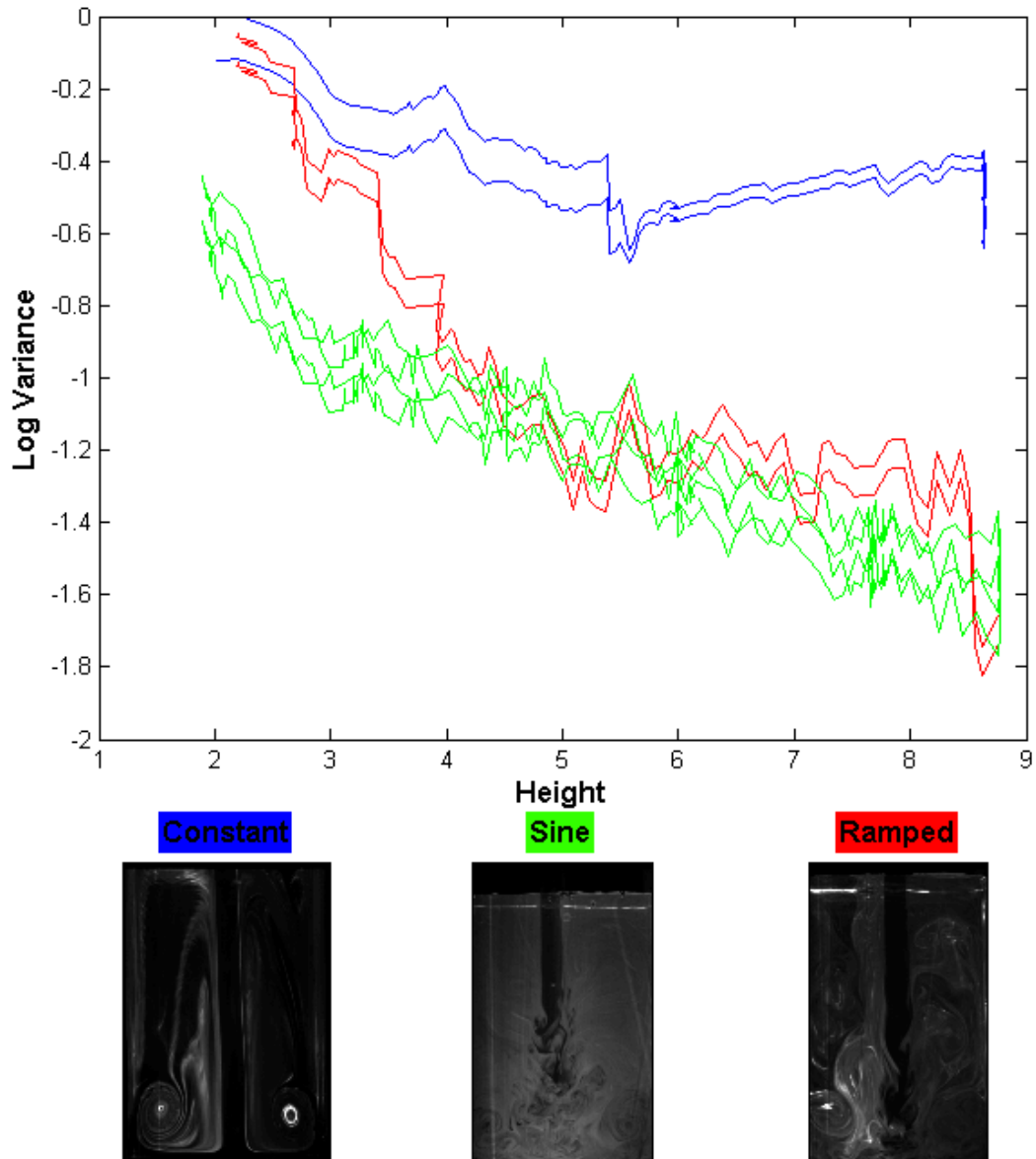
Figure 6.1 Mixing performance for three nozzles at a viscosity of 18 mPa s (a) log variance plotted against fluid height (cm); Image of the vessel filled with (b) constant flow rate of $Q = 3.33 \times 10^{-5} m^3 s^{-1}$ (c) sinusoidal flow rate varying between $1.67 \times 10^{-5} m^3 s^{-1}$ and $5 \times 10^{-5} m^3 s^{-1}$ (d) flow rate increasing from 0 to $6.67 \times 10^{-5} m^3 s^{-1}$

Figure 6.1 shows the log variance of these two scenarios next to a case with constant flow rate at the average flow rate for each case ($3.33 \times 10^{-5} m^3 s^{-1}$), the case at constant flow rate reaches a log variance of -0.6 which is 50% mixed . Both the sine and the ramped flow result in a marked improvement in the level of mixing within the

tank. For the ramped flow the low flow rate at the beginning of the fill means the decrease in the log variance is more gradual throughout the process, the log variance reaches approximately -1.4 which is 80% mixed. In contrast the sine function reaches a log variance of -1.6 which 84% mixed. Figures 6.1c and 6.1d confirm this, the sine case appears to be more homogeneous than the ramped case, however both are a large improvement on figure 6.1b in which little mixing has taken place.

6.3   Nozzle improvements

The obstruction at the end of the pipe seen in section 4.3.2 resulted in a great improvement in the level of mixing seen. To replicate this two nozzles were built with a cone insert in the base as described in section 3.2.3. A third nozzle with a swirl insert was also investigated; this nozzle was designed to give the jet angular momentum so it would spread to greater regions of the tank.

Figure 6.2 shows the log variance achieved in the tank for the two cone nozzles in comparison with the simple straight flow that reaches 50% mixed. The mixing performance has dramatically improved. The second cone which is the smaller of the two shows the best improvement in the mixing performance reaching a log variance of -1.7 (86% mixed), however due to the level of noise in the log variance signal it is difficult to differentiate between the two cases. Comparison of the images in Fig 6.2.c and Fig 6.2.d does indicate that the smaller nozzle has produced a more homogeneous vessel.

Figure 6.2 Mixing performance for three nozzles at a fill rate of Q = 3.33×10⁻⁵ m³ s⁻¹ and a viscosity of 18 mPa s (a) log variance plotted against fluid height (cm); Image of the vessel filled with (b) straight pipe (c) cone 1 nozzle (d) cone 2 nozzle

Figure 6.3 shows the improvement achieved using a swirl nozzle, this nozzle provides a much greater improvement than the cone nozzles with the log variance reaching -2.6 (95% mixed) at points in the fill. Figure 6.3c shows that the fluid in the tank is much more homogeneous than in Figures 6.2c and 6.2d. It appears that the angular momentum applied to the fluid by the swirl insert in the end of the nozzle has

increased the level of mixing particularly in the top half of the tank, by directing the

flow towards these stagnant regions.

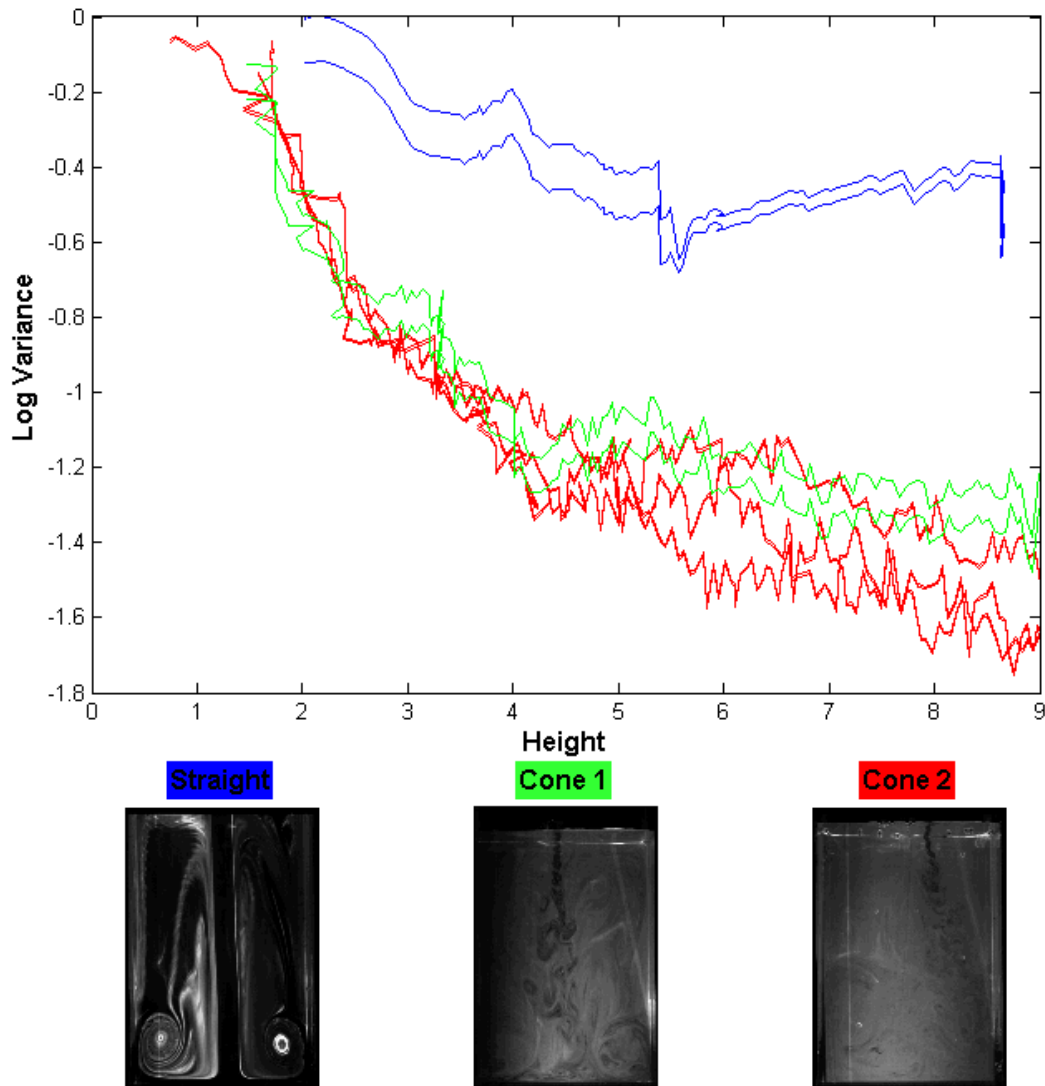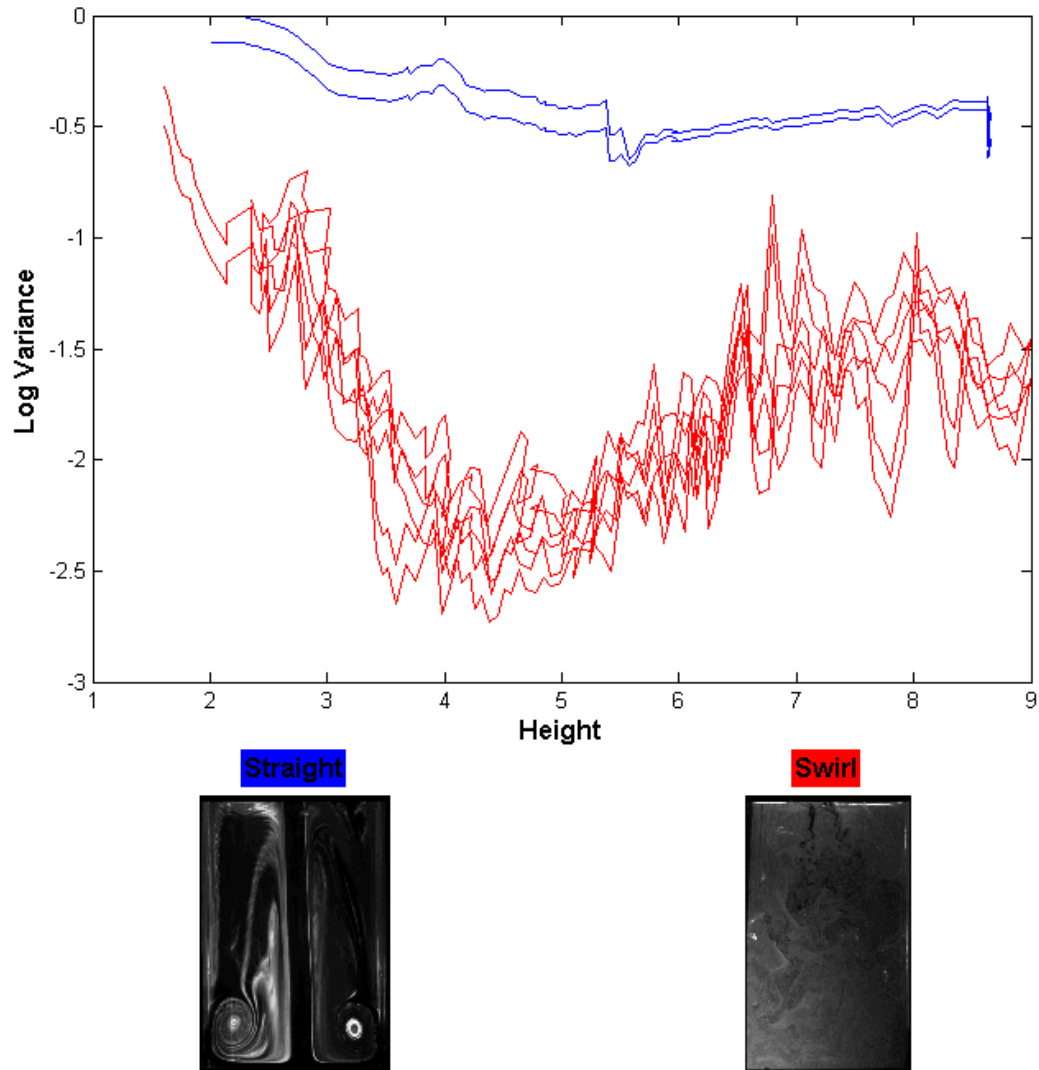*Figure 6.3   Mixing performance for two nozzles at a fill rate of Q = 3.33×10^{-5} m^3 s^{-1}and a viscosity of*

18 mPa s (a) log variance plotted against fluid height (cm); Image of the vessel filled with (b) straight

pipe (c) swirl nozzle

6.4   Conclusions

Improvements to the mixing performance have been made by both changing the inlet pipe geometry and varying the inlet flow rate. Two flow rate variations were investigated, ramped flow and a sinusoidal flow, the sinusoidal function variations in the inlet velocity increased the level of mixing from 50% mixed so that the vessel reached 84% mixed. Changing the nozzle design had a greater effect on the level of mixing, three nozzle designs were examined, the most successful of these had a swirl insert in the bottom of the pipe. With the swirl insert the level of mixing in the tank reached 95% (log variance of -2.6) at one point in the fill, however this was not maintained throughout. To further improve the mixing it may be beneficial to combine these improvements, such as by using a sinusoidal flow rate through a swirl nozzle. This may produce a more sustained and reliable improvement and should feature in any future work.

Chapter 7 Conclusions

7.1   Mixing in a filling vessel

There is a large body of work into mixing by a range of mechanisms, however very little has been carried out on the mixing that occurs as a vessel is filled. This mixing process has been investigated using the techniques PLIF and PIV. These techniques have been used to measure a variety of flow scenarios in the literature, however in most cases the system is a steady state. This work has adapted these techniques to measure the mixing of transient systems with a moving free surface.

The PLIF technique has been demonstrated to give good repeatability for the same flow conditions and qualitative examination of the images has revealed a change in the mixing mechanism from laminar to turbulent above a critical value of the Reynolds number (Re~1000) which agrees with previous literature. For the cases with a retracting pipe above Re~1000 the log variance reaches -2.2 in each case which equates to 92% mixed.

PIV was used to measure the vector fields in the tank, allowing the distribution of momentum and shear in the tank to be investigated. For all flows dead regions were observed in the bottom corners of the tank and the top half of the tank was relatively quiescent, however this was more prominent for more laminar flows. For the more turbulent flows (Re > 1000) there was a higher level of movement in the top half of the tank. To improve the mixing performance in the laminar cases this movement must be created and accentuated, changes to the flow rate and the nozzle design were made to achieve this.

Sinusoidal function variations in the inlet velocity increased the level of mixing from an unmixed highly striated case so that the vessel reached 84% mixed, however changing the nozzle design had a greater effect on the level of mixing. Three nozzle designs were examined, the most successful of these had a swirl insert in the bottom of the pipe. With the swirl insert the level of mixing in the tank reached 95% (log variance of -2.6) at one point in the fill, however this was not maintained throughout. To further improve the mixing it may be beneficial to combine these improvements, such as by using a sinusoidal flow rate through a swirl nozzle. This may produce a more sustained and reliable improvement and should feature in any future work.

7.2   Future work

PLIF has proven to be a useful tool in measuring the mixing within a filling tank, the development of the mixing analysis allows this technique to be used for other systems with moving free surfaces.

There are a number of avenues that can be explored to improve the mixing in the tank further; combining the variable flow rate with the nozzle design changes, changing the tank geometry, adding internal baffles to the tank, adding the variant and the base product simultaneously, or mixing in the nozzle. There are also a number of challenges to overcome in translating the understanding of the Newtonian mixing and flow patterns into rules that will work with real products.

One option for the screening of different improvements to the flow is the use of Computational Fluid Dynamics, however its application requires a number of

challenges to be overcome. The first is the difficulties in solving a flow with such high viscous stresses and the accuracy of the results obtained, as the pressure correction solver in the commercially available code often assumes that the viscous stresses are much smaller than the inertial stresses. Furthermore while the mixing in the tank can be modelled using the commercially available solvers the accuracy is greatly dependent on the mesh. A very fine mesh is required as the lengthscale of the mixing can only be determined down to the size of the mesh being used. Also the mesh quality has to be high with predominantly hexahedral elements, and the time step must be carefully chosen to reduce the numerical diffusion. These factors can lead to long run times which reduces the effectiveness of CFD as a screening tool.

It would be a useful measure of the mixing improvement, gained through the nozzle and flow rate changes made in this thesis, to test the techniques on real products. Limited understanding of the flow structure would be gained due to the opaque nature of the product but the level of mixing in the bottle can be measured using a dye and measuring the colour of the resulting liquid. This would allow a correlation between the Newtonian PLIF results and the real product to be made.

References

Bi, W., Sugii, Y., Okamoto, K., Madarame, H. (2003) "Time-resolved proper orthogonal decomposition of near-field flow of a round jet measured by dynamic particle image velocimetry" *Measurement Science and Technology* 14 L1-L5

Bin, A. K. (1988). "Minimum air entrainment velocity of vertical plunging liquid jets." *Chemical Engineering Science*, 43(2), 379-389.

Brown, D. A. R., Jones, P. N., and Middleton, J. C.(2004). "Experimental methods." In: *Handbook of industrial mixing: science and practice*, Paul E.L., Atiemo-Obeng V.A., and Kresta S.M., eds., John Wiley & Sons Inc., New Jersey, 145-256.

Chen, Y. C., Ma, C. F., Qin, M., and Li, Y. (2005). "Theoretical study on impingement heat transfer with single-phase free-surface slot jets." *International Journal of Heat and Mass Transfer*, 48(16), 3381-3386.

Chung, K. H. K., Barigou, M., and Simmons, M. J. H. (2006). "Reconstruction of 3-D flow field inside miniature stirred vessels using a 2-D PIV technique." 12th European Conference on mixing.

Cozewith, C., and Busko, M. (1989). "Design Correlations for Mixing Tees." *Industrial & Engineering Chemistry Research*, 28(10), 1521-1530.

Dazin, A., Dupont, P., and Stanislas, M. (2006). "Experimental characterization of the instability of the vortex ring. Part I: Linear phase." *Experiments in Fluids*, 40(3), 383-399.

Degardin, O., Renou, B., and Boukhalfa, A. M. (2006). "Simultaneous measurement of temperature and fuel mole fraction using acetone planar induced fluorescence and Rayleigh scattering in stratified flames." *Experiments in Fluids*, 40(3), 452-463.

Ding, R., Revstedt, J., Fuchs, L. (2003) "LIF Study of Mixing in Circular Impinging Jets; Effects of Boundary Conditions" *Proceedings of PSFVIP-4, Chamonix, France* F4015

Etchells, A.W., Meyer, C.F. (2004). " Mixing in pipelines." In: *Handbook of industrial mixing: science and practice*, Paul E.L., Atiemo-Obeng V.A., and Kresta S.M., eds., John Wiley & Sons Inc., New Jersey, Ch 7, 391 - 478.

Fall, A., Lecoq, O., and David, R. (2001). "Characterization of mixing in a stirred tank by planar laser induced fluorescence (PLIF)." *Chemical Engineering Research & Design*, 79(A8), 876-882.

Feng, H., Olsen, M. G., Liu, Y., Fox, R. O., and Hill, J. C. (2005). "Investigation of turbulent mixing in a confined planar-jet reactor." *Aiche Journal*, 51(10), 2649-2664.

Fondse, H., Leijdens, H., and Ooms, G. (1983). "On the Influence of the Exit Conditions on the Entrainment Rate in the Development Region of A Free, Round, Turbulent Jet." *Applied Scientific Research*, 40(4), 355-375.

Fosset, H., Prosser, L. E., (1949). "The application of free jets to mixing of fluids in bulk." Proceedings of the Institute of Mechanical Engineers. 160, 224-232

Forney, L. J., and Lee, H. C. (1982). "Optimum Dimensions for Pipeline Mixing at A T-Junction." *Aiche Journal*, 28(6), 980-987.

Golnabi, H. (2006). "Precise CCD image analysis for planar laser-induced fluorescence experiments." *Optics and Laser Technology*, 38(3), 152-161.

Grenville, R.K., Nienow, A.W. (2004). " Blending of miscible liquids." In: *Handbook of industrial mixing: science and practice*, Paul E.L., Atiemo-Obeng V.A., and Kresta S.M., eds., John Wiley & Sons Inc., New Jersey, Ch 9, 507 - 542.

Guillard, F., Fritzon, R., Revstedt, J., Tragardh, C., Alden, M., and Fuchs, L. (1998). "Mixing in a confined turbulent impinging jet using planar laser-induced fluorescence." *Experiments in Fluids*, 25(2), 143-150.

Guillard, F., Tragardh, C., and Fuchs, L. (2000). "A study on the instability of coherent mixing structures in a continuously stirred tank." *Chemical Engineering Science*, 55(23), 5657-5670.

Hall, J. F., Barigou, M., Simmons, M. J. H., and Stitt, E. H. (2004). "Mixing in unbaffled high-throughput experimentation reactors." *Industrial & Engineering Chemistry Research*, 43(15), 4149-4158.

Hall, J. F., Barigou, M., Simmons, M. J. H., and Stitt, E. H. (2005). "Comparative study of different mixing strategies in small high throughput experimentation reactors." *Chemical Engineering Science*, 60(8-9), 2355-2368.

Houcine, I., Vivier, H., Plasari, E., David, R., and Villermaux, J. (1996). "Planar laser induced fluorescence technique for measurements of concentration fields in continuous stirred tank reactors." *Experiments in Fluids*, 22(2), 95-102.

Hult, J., Meier, U., Meier, W., Harvey, A., and Kaminski, C. F. (2005). "Experimental analysis of local flame extinction in a turbulent jet diffusion flame by high repetition 2-D laser techniques and multi-scalar measurements." *Proceedings of the Combustion Institute*, 30, 701-709.

Kim, K. C., Min, Y. U., Oh, S. J., An, N. H., Seoudi, B., Chun, H. H., and Lee, I. (2007). "Time-resolved PIV investigation on the unsteadiness of a low Reynolds number confined impinging jet." *Journal of Visualization*, 10, 367-379.

Kresta, S. M., Brodkey, R.S. (2004). "Turbulence in Mixing Applications." In: *Handbook of industrial mixing: science and practice*, Paul E.L., Atiemo-Obeng V.A., and Kresta S.M., eds., John Wiley & Sons Inc., New Jersey, Ch 2, 19 – 87.

Kresta, S. M., Wood, P.E. (1993). "The flow field produced by a pitched blade turbine:characterisation of the turbulence and estimation of the dissipation rate." *Chemical Engineering Science*, 48, 1761-1774

Kukukova, A., Aubin, J., and Kresta, S. M. (2009). "A new definition of mixing and segregation: Three dimensions of a key process variable." *Chemical Engineering Research & Design*, 87(4A), 633-647.

Lane, A. G. C., and Rice, P. (1982). "Comparative-Assessment of the Performance of the 3 Designs for Liquid Jet Mixing." *Industrial & Engineering Chemistry Process Design and Development*, 21(4), 650-653.

Law, A. W. K., and Wang, H. W. (2000). "Measurement of mixing processes with combined digital particle image velocimetry and planar laser induced fluorescence." *Experimental Thermal and Fluid Science*, 22(3-4), 213-229.

Mortensen, M., Orciuch, W., Bouaifi, M., and Andersson, B. (2004). "Mixing of a jet in a pipe." *Chemical Engineering Research & Design*, 82(A3), 357-363.

Neal, G., Simmons, M. J. H., Hough, J. A., and Fryer, P. J. (2008). "Criteria for measuring mixing performance in a vessel with a rising free surface." *Experiments in Fluids*, 45: 3-12.

Neal G.., Simmons M.J.H., Hough J.A., Fryer P.J. (2008) "Mixing in a vessel with a rising free surface" *Proceedings of the International symposium on mixing in industrial processes (ISMIP 2008),*

Neal G., Simmons M.J.H., Hough J.A., Fryer P.J. (2009) "Mixing in a vessel with a rising free surface" *Proceedings of the World Congress in Chemical Engineering 2009.*

Ottino, J. M., (1989). *The kinematics of mixing: stretching, chaos, and transport* Cambridge University Press, Cambridge.

Pan, G., and Meng, H. (2001). "Experimental study of turbulent mixing in a tee mixer using PIV and PLIF." *Aiche Journal*, 47(12), 2653-2665.

Patwardhan, A. W., and Gaikwad, S. G. (2003). "Mixing in Tanks Agitated By Jets." *Trans IChemE*, 81(A), 211-220.

Paul, E.L., Atiemo-Obeng, V.A., and Kresta S.M. (2004). "Introduction" In: *Handbook of industrial mixing: science and practice*, Paul E.L., Atiemo-Obeng V.A., and Kresta S.M., eds., John Wiley & Sons Inc., New Jersey.

Pawlak, G., Cruz, C. M., Bazan, C. M., and Hrdy, P. G. (2007). "Experimental characterization of starting jet dynamics." *Fluid Dynamics Research*, 39, 711-730.

Raffel, M., Willert, C. E., Wereley, S. T., and Kompenhans, J. (2007). *Particle Image Velocimetry, A Practical Guide*, Second Edition Ed., Springer.

Reungoat, D., Riviere, N., and Faure, J. P. (2007). "3C PIV and PLIF measurement in turbulent mixing - Round jet impingement." *Journal of Visualization*, 10(1), 99-110.

Revill, B. K. (1985). "Jet Mixing." In: *Mixing in the process industries*, Harnby, N., Edwards, M.F., Nienow, A.W., eds., Butterworths, 145 -169.

Saarenrinne, P., Piirto, M., Eloranta, H., (2001) "Experiences of turbulence measurement with PIV," Measurement Science Technology 12, 1904

Szalai, E. S., Alvarez, M. M., Muzzio, F. J. (2004). " Laminar mixing: A dynamical approach." In: *Handbook of industrial mixing: science and practice*, Paul E.L., Atiemo-Obeng V.A., and Kresta S.M., eds., John Wiley & Sons Inc., New Jersey, Ch 3, 89 - 144.

Unger, D. R., and Muzzio, F. J. (1999). "Laser-induced fluorescence technique for the quantification of mixing in impinging jets." *Aiche Journal*, 45(12), 2477-2486.

Unger, D. R., Muzzio, F. J., and Brodkey, R. S. (1998). "Experimental and numerical characterization of viscous flow and mixing in an impinging jet contactor." *Canadian Journal of Chemical Engineering*, 76(3), 546-555.

Weigand, P., Meier, W., Duan, X. R., Stricker, W., and Aigner, M. (2006). "Investigations of swirl flames in a gas turbine model combustor - I. Flow field, structures, temperature, and species distributions." *Combustion and Flame*, 144(1-2), 205-224.

Weisgraber, T. H., and Liepmann, D. (1998). "Turbulent structure during transition to self-similarity in a round jet." *Experiments in Fluids*, 24(3), 210-224.

Zughbi, H. D., and Ahmad, Q. (2005). "Mixing in liquid-jet-agitated tanks: Effects of jet asymmetry." *Industrial & Engineering Chemistry Research*, 44(4), 1052-1066.

Zughbi, H. D., and Rakib, M. A. (2004). "Mixing in a fluid jet agitated tank: effects of jet angle and elevation and number of jets." *Chemical Engineering Science*, 59(4), 829-842.

Appendix: Matlab analysis code

PLIF Analysis Script

```
T=6; %the width of the tank in cm
R=8; %the mg of Rhodamine in 1 ml put in bottom of vessel initially
Irange=(31:199); % image range
vbase=1003; %vessel base cut off
vleft=200; % vessel left cut off
vright=647; %vessel right cut off
inletleft=189;%the position of the inlet pipe in relation to the tank
inletright=279;
heightlogsigma=zeros(length(Irange),3);
size=zeros(length(Irange),2);

[M,K]=fcalibration(R,T);

for count=1:length(Irange)
    cd 'E:\Experiments\0606PLIF8\4run\Image\Single' %the directory with the images in it
    I=zeros(1016,1000);
    I=imread (sprintf('4run0%04.4d.tif',Irange(count))); %reads the images
    cd 'E:\mfiles' %changes to the directory with the mfiles in it
    [A,Mi,Ki]=ffluidarea(I,vbase,vleft,vright,M,K);
    clear I
    [Cinf,H]=finfconc(A,R,Mi,Ki,T);
    [C1,C2]=fnormconc(A,Ki,Cinf,inletleft,inletright);
    clear A Cinf
    [V,E]=flogsigmaRMS(C1,C2);
    heightlogsigma(count,1)=H;
    heightlogsigma(count,2)=V(1,1);
    heightlogsigma(count,3)=V(1,2);
    size(count,1)=E(1,1);
    size(count,2)=E(1,2);
    clear V Mi Ki C
    count=count+1;
end

clear count M K T R Irange vbase vright vleft inletleft inletright

plot(heightlogsigma(:,1),heightlogsigma(:,2),'r',heightlogsigma(:,1),heightlogsigma(:,3),'b')
```

Associated functions

```
function [M,K,I]=fcalibration(R,T)
%a function to give the gradient and intercept of graph relating the
%concentration to the greyscale.  The output is two mattrices with these
%values for each pixel in the field.

cd 'E:\Experiments\0606PLIF8\cal\Image\Single'

irange1=(0:49);%input('enter cal image numbers for 1 dose:\n');
irange2=(50:99);%(input('enter cal image numbers for 2 dose:\n');
height=11.4;%input('enter height of liquid in calibration images:\n');

I=imread (sprintf('cal0%04.4d.tif',irange1(1)));
for count=2:length(irange1);
   I1=imread (sprintf('cal0%04.4d.tif',irange1(count)));
   I=cat(3,I,I1);
   clear I1
   count=count+1;
end

I1=mean(I,3);
clear I

I=imread (sprintf('cal0%04.4d.tif',irange2(1)));
for count=2:length(irange1);
   I2=imread (sprintf('cal0%04.4d.tif',irange2(count)));
   I=cat(3,I,I2);
   clear I2
   count=count+1;
end

I2=mean(I,3);
%clear I

K=2*I1-I2;

Conc=R/(T*T*height);
M=(I2-I1)/Conc;

function [A,Mi,Ki]=fluidarea(I,vbase,vleft,vright,M,K)
%program for focusing on the area that contains fluid in the
%vessel described in image I.  This function takes the image determines the
%area with a greyscale 10% higher than the background greyscale and outputs
%a mattrix with greyscale values for the fluid area.  It then scales the
%concentration gradient and intercept so that they are mattrices of the
%correct size.

B=mean(I(:,2));
cutoff=mean(B)+0.07*mean(B); %determines greyscale cut off value
%cutoff=77;

G=I(1:vbase,vleft:vright); % cuts off side and base of fluid
```

```
F=mean(G');
E=find(F>cutoff);%creates vector containing the rows above the cut off greyscale

A=G(min(E)+30:vbase,:);
Mi=M(min(E)+30:vbase,vleft:vright);%cuts the gradient matrix to size
Ki=K(min(E)+30:vbase,vleft:vright);%cuts the intercept matrix to size
end

function [Cinf,H]=infconc(A,Cinit,M,K,T)
%function to deterime what the final greyscale would be if the vessel was
%well mixed at that fill height.  A is the fluid area as defined by the
%fluid area function, Cinit is the concentration of the 1ml of tracer
%intially placed in the bottom of the tank in mg.  M is the gradient and K the
%intercept of the linear relationship between concentration(x)and greyscale(y),
%T is the tank width in centimetres.

[B,D]=size(A); % tells us the no of rows (B) and the number of columns (D)

H=(B+30)*(T/D); % gives us the height of the liquid in centimetres

V=T*T*H; %the volume of fluid in the tank in ml

C=Cinit/V; %the concentration in the tank

Cinf=C*M+K; %calculates the infinite concentration greyscale value at that height

end

function [C1,C2]=normconc(A,Czero,Cinf,inletleft,inletright);
%outputs a normalised concentration - Cinf is the greyscale that the
%vessel would be at if completely mixed at the fill height of that image,
%Czero is the greyscale value when the concentration is zero, A is the area
%of fluid that has been previously determined by the fluid area function

B=double(A);

Dt=(B-Czero);
Du=(Cinf-Czero);

Ct1=Dt(:,1:inletleft);
Ct2=Dt(:,inletright:end);
Cu1=Du(:,1:inletleft);
Cu2=Du(:,inletright:end);

Ct1=Ct1(:);
Cu1=Cu1(:);

y=find(Cu1<2);
Ct1(y)=[];
Cu1(y)=[];
C1=Ct1./Cu1;

Ct2=Ct2(:);
Cu2=Cu2(:);
```

```
y=find(Cu2<2);
Ct2(y)=[];
Cu2(y)=[];
C2=Ct2./Cu2;

end

function [V,E]=logsigmaRMS(C1,C2)
%function to determine the log of the RMS variance, C is the normalised
%concentration mattrix

A1=C1-1;
A2=C2-1;

B1=A1.^2;
B2=A2.^2;

D1=sum(B1);
D2=sum(B1);
E1=length(B1);
E2=length(B2);

D=[D1,D2];
E=[E1,E2];

V=log(D./E);

end
```

PIV Analysis Script

```
cd ('F:\PIV\graceeee\3ml02car7J\Analysis');

range1=00:299;

A=csvread
(sprintf('3ml02car7J00%04.4d.T000.D000.P001.H001.L.vec',range1(1)),1,0);%front vector
file behind which the others are stacked
l=2;
for l=2:length(range1)
   B=csvread (sprintf('3ml02car7J00%04.4d.T000.D000.P001.H001.L.vec',range1(l)),1,0);
   A=cat(3,A,B);
   l=l+1;
end
clear B

cd ('F:\mfiles');

%remove false values
[D,L]=find(A(:,5,:)<1);%finds all where 'false' is indicated by the software
for l=1:length(D);
   A(D(l),3:5,L(l))=0;%sets the velocities and the 5th column to zero for the false vectors
   l=l+1;
end
%remove false x velocity values
j=1;
[D,L]=find(abs(A(:,3,:))>20);%finds all where x velocity is greater that 2m/s-unrealistic in
this flow context
for j=1:length(D);
   A(D(j),3:5,L(j))=0;%sets the velocities and the 5th column to zero for the false vectors
   j=l+1;
end
%remove false y velocity values
j=1;
[D,L]=find(abs(A(:,4,:))>20);%finds all where y velocity is greater that 2m/s-unrealistic in
this flow context
for j=1:length(D);
   A(D(j),3:5,L(j))=0;%sets the velocities and the 5th column to zero for the false vectors
   j=l+1;
 end

%time average velocity
ubar=zeros(size(A,1),5);
B=sum(A,3);%sums all the velocities
ubar(:,1:2)=A(:,1:2,1);%sets the position vectors so they are the same as the orginal
ubar(:,3:4)=B(:,3:4)./(B(:,5)*ones(1,2));%gives average velocity by dividing sum by number
of valid vectors
ubar(:,5)=B(:,5);
clear B

%root mean square
l=1;
B=A;
```

```
for l=1:(size(A,3))
    B(:,3:4,l)=(A(:,3:4,l)-ubar(:,3:4)).^2;
    l=l+1;
end

for l=1:length(D);
    B(D(l),3:5,L(l))=0;%resets the velocities and the 5th column to zero for the false vectors
    l=l+1;
end
C=sum(B,3);
urms2=C(:,3:4)./(C(:,5)*ones(1,2));%where this is the rms value squared

clear B C l
clear D L

%TKE
k=ones(length(A),3);
k(:,1:2)=A(:,1:2,1);
k(:,3)=0.75*(urms2(:,1).*urms2(:,2));

%reorganise for plotting!
d=find(k(:,2)<k(1,2));
e=length(k)/(min(d)-1);
K=reshape(k(:,3),(min(d)-1),e);
K=K';

c=min(ubar(:,1));
b=max(ubar(:,1));
f=min(ubar(:,2));
g=max(ubar(:,2));
lim=[c-0.5 b+0.5 f-0.5 g+0.5];

clear k d e c b f g

%code to create average ubar, velocity magnetude field, and contour plot,
ubarg=ubar9J;
ubarj=ubar9g;
kj=K9g;
K=K9J;

limit=1.4;%speed in m/s of the cutoff point between the two versions of ubar and K;

U=(ubarg(:,3).^2+ubarg(:,4).^2).^0.5;%0.5; give column with average speed

B=find(U>limit);

ubar=ubarg;
for l=1:length(B);
    ubar(B(l),:)=ubarj(B(l),:);
    l=l+1;
end

ubar=ubar./10;
U=(ubar(:,3).^2+ubar(:,4).^2).^0.5;%0.5; give column with average speed with jet values for
larger numbers
```

```
U=reshape(U,size(K'));

B=find(U>limit);
K=K';
for l=1:length(B);
   K(B(l))=kj(B(l));
   l=l+1;
end

K=K'./100;
U=U';
K=flipud(K);
U=flipud(U);

contour(U)
```